九州大学学術情報リポジトリ
Kyushu University Institutional Repository

Measurements of PVT and Vapor-Liquid Equilibrium Properties of Low Global-Warming-Potential Refrigerants

江, 世恒

https://hdl.handle.net/2324/1959127

出版情報：Kyushu University, 2018, 博士（工学）, 課程博士
バージョン：
権利関係：

Measurements of PVT and Vapor-Liquid Equilibrium Properties of Low Global-Warming-Potential Refrigerants

Ph.D. Thesis

Shiheng Jiang

Department of Mechanical Engineering

Graduate School of Engineering

Kyushu University

Japan

2018

Contents

Nomenclature iv

Chapter 1 Introduction 1

1.1 Background 1

1.2 Refrigerants 2

1.2.1 First generation 3

1.2.2 Second generation 4

1.2.3 The third generation 5

1.2.4 The fourth generation 7

1.2.5 Numbering scheme 8

1.3 Literature review 10

1.3.1 Thermodynamic properties of R1234ze(Z) 10

1.3.2 Thermodynamic properties of R1234yf and the binary mixtures with other refrigerants 12

1.3.3 Thermodynamic properties of R1123 and the binary mixture with R32. 16

1.4 Thesis objective 18

1.5 Thesis outline 19

Chapter 2 Burnett Method 21

2.1 Introduction 21

2.2 Fundamental equations 22

2.3 Experimental apparatus 23

2.3.1 Schematic diagram of the experimental devices 23

2.3.2 Pressure vessels 25

2.3.3 Isothermal bath and SPRT 25

2.3.4 Modification of the pressure transducer 28
2.4 Experimental procedure..... 29
2.4.1 Steps of measurement 29
2.4.2 Supplying method for R1234ze(Z) 30
2.5 Uncertainties of experimental data 32
Chapter 3 Vapor-Liquid Equilibrium Measurement 33
3.1 Experimental apparatus 33
3.1.1 Outline of the experimental facilities..... 33
3.1.2 Structure inside the thermostat bath..... 34
3.1.3 Temperature control system 35
3.1.4 Temperature measurement 36
3.1.5 Extraction system..... 37
3.1.6 Gas chromatograph 38
3.2 Correlation between the area ratio and concentration 39
3.2.1 R32 + R1123 39
3.2.2 R32 + R1234yf..... 40
3.2.3 R1123 + R1234yf..... 41
3.4 Uncertainties..... 42
Chapter 4 Experimental Results on PVT Properties 43
4.1 PVT property measurements for helium 44
4.1.1 Experimental results..... 44
4.1.2 Comparisons with the EOS by Ortiz-Vega et al..... 47
4.2 PVT properties measurements for nitrogen..... 48
4.2.1 Experimental results..... 48
4.2.2 Comparisons with the EOS by Span et al. 51
4.3 PVT properties measurements for R134a..... 52
4.3.1 Experimental results..... 52

4.3.2 Comparisons with Tillner-Roth and Baehr's EOS 55
4.4 PVT properties measurement for R1234ze(Z) 56
4.4.1 Experimental results..... 56
4.4.2 Comparisons with other published data and the EOS by Akasaka et al. 59
Chapter 5 Experimental Results on VLE Properties 62
5.1 VLE properties for binary mixture of R32 + R1234yf 62
5.1.1 Experimental results..... 62
5.1.2 Comparisons with the EOS and other published data..... 63
5.2 VLE properties for the binary mixture of R32 + R1123 65
5.2.1 Experimental results..... 65
5.2.2 Comparisons with the EOS with default mixing parameters..... 66
5.3 VLE properties for the binary mixture of R1123 + R1234yf 69
5.3.1 Experimental results..... 69
5.3.2 Comparison with the EOS with default mixing parameters 69
5.4 Discussion..... 72
Chapter 6 Conclusions..... 76
Reference 80
Acknowledgement 88

Nomenclature

P	Pressure
P_{EOS}	Calculated pressure by EOS
P_{EXP}	Experimental pressure
Z	Compressibility factor
V	Volume
V_A	Volume of sample cell
V_B	Volume of expansion cell
R	Gas constant
m	Mass
N	Cell constant
k	Coverage factor
y	Concentration
y_{mass}	Mass fraction
x	Area ratio of peaks
U	Uncertainty
k_{ij}	Interaction parameters

Greek symbols

ρ	Density
ω	Acentric factor

Chapter 1 Introduction

1.1 Background

Since 1980, the earth's surface temperature rises at a step of average 0.74 K per year and in the 21st century the coldest year (2008) was warmer than all the years in the 20th century except for 1998. [1] The phenomenon of this climate change called global warming which is observed in the scale of century will cause enormous effect on the environment of human habitation. Although the periodic motion of the earth and the sun will cause climate change, the human activities such as emissions of greenhouse gases are also considered as a significant factors to accelerate the warming rate which is almost double in the last half century. Therefore some societal should response to global warming problem like mitigation by emissions reduction.

In the recent decades, the hydrofluorocarbons (HFCs) become the most widely used refrigerants which are known as nonozone depleting agents. However the greenhouses effect of these kinds are also substantial and their global warming potential (GWP) values are hundreds or thousands times larger than the carbon dioxide. To achieve the goal of emissions reduction of greenhouse gases, a global agreement signed in Kigali recently to limit the use of HFCs starting by 2019. Consequently, new active area of research has been promoted toward the development of low GWP new refrigerants. Hydrofluoroolefins (HFOs) have been synthesized as a low GWP alternative to the third generation HFC refrigerants, but some HFOs have the problem of flammability. In order to maintain the safety of home refrigerators and air-conditioners, mixing a small amount of HFCs with HFOs may be effective.

The further study on fully characterizing them and their blends with other compounds is still required to fully assess their performance to replace the ones in current

use. The understanding of thermodynamic properties behavior of new refrigerants are of great importance as fundamental information for developing industrial equipment working fluids such as heat pump systems, organic Rankine cycles and refrigerators. In this study, an expansion method also called Burnett method was applied to measure the PVT properties. The apparatus has been developed and verified by measuring some substances which have published data and equation of state. The PVT properties of new low GWP refrigerant cis-1,3,3,3-tetrafluoropropene (R1234ze(Z)) have been measured at temperature from 353 K to 413 K. For the vapor-liquid equilibrium properties, binary mixture as shown in the Fig 1.1 of difluoromethane (R32), trifluoroethylene (R1123) and 2,3,3,3-tetrafluoroprop-1-ene (R1234yf) have been measured at temperature from 273 K to 313 K.

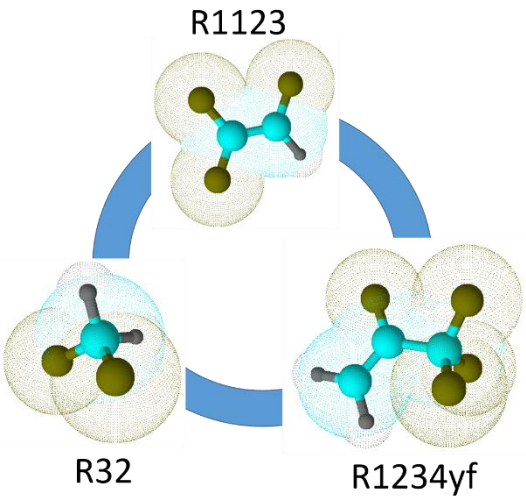

Figure 1.1 Binary mixtures of next generation of refrigerants in this study

1.2 Refrigerants

In the ancient times, human beings utilized the ice, vaporization of water, and other evaporation process to achieve the goal of refrigeration. From 1600s to 1700s, plenty of researches about phase change had been done in different countries to establish the foundation for artificial refrigeration. In 1830s, Perkins [2] invented the first vapor-

compression machine. To commemorate Perkins' distinguished work, the mechanical vapor-compression approach is identified as the Perkins Cycle. Since then the time of the development of the refrigerants arrived. According to James M. Calm et al. (2008) [3] description, the development of the refrigerants can be divided into 4 generations as shown in the Table 1.1.

Table 1.1 Generations of the refrigerants

	1th generation	2nd generation	3rd generation	4th generation
Times	1830 ~ 1930	1931 ~ 1990	1991 ~ 2010	2010 ~ Present
Refrigerants	CO_2, NH_3, SO_2, H_2O, Air	CFCs, HCFCs, NH_3, H_2O	HFCs, NH_3, HCs, CO_2	HFOs, NH_3. HCs, CO_2

1.2.1 First generation

From 1830s to 1930s, almost all kinds of refrigerants were flammable, toxic, or both, and some had the potential of strong chemical reaction [4]. The only way to determine whether one substance can be utilized as refrigerant was if it can work. During this period, many kinds of technology of refrigeration were studied. The applications of steam compression refrigerators, air circulation refrigerators, absorption refrigerators and water evaporative refrigerators had worked through nearly the whole one hundred years.

Originally, the methyl ether (RE170) was applied in steam compression refrigerator. Later period, ammonia (R717), carbon dioxide (R744), sulfur dioxide (R764) and chloromethane (R40) were applied. Especially, the development of utilizing the ammonia had promptly evolved the technology of this refrigerator. Around 1900s, the USA, England and German had promoted updating the refrigerants to ammonia and carbon dioxide [5].

The absorption refrigerator used ammonia water to produce ice. While the process of sulfur dioxide absorbing vapor water was applied in the water evaporative refrigerator to produce ice.

1.2.2 Second generation

Compared with the first generation, the second generation had better safety and durability. From 1931 to 1990, the fluorochemicals, one kind of the halohydrocarbon (CFCs, HCFCs), became the major refrigerants all over the world. The new refrigerants with the properties shown in the Table 1.2 [4, 6] of non-toxic and incombustibility (A1) had satisfied the demand of the increasing air conditioning industry for over 60 years. For the second generation, the ammonia was still applied due to the low price and the excellent thermodynamic property. [7] However the market shares of the ammonia was gradually decreasing because of the toxicity and pungent penetrating odor.

Among the second generation, the R12 was widely utilized in the household refrigerator, cabinet freezer and display cabinet. In addition, the R12 was the only refrigerant in the vehicle air conditioner. The R22 was applied in household air conditioner, large-scale heat pump. The R11 was used in large scale centrifugal water chiller.

Table 1.2 The second generation of refrigerants [4, 6]

Refrigerants	Category	Safety	ODP
R12	CFC	A1	1.0
R11	CFC	A1	1.0
R114	CFC	A1	0.6
R113	CFC	A1	0.8
R22	HCFC	A1	0.055
R13	CFC	A1	1.0

1.2.3 The third generation

After 1970s, people realized that the CFCs did harm to the ozone in the stratosphere and caused the ozonosphere hole over the Antarctica. The oxygen reactions [8] in the atmosphere can be expressed as the following formulas, so called Chapman cycle:

$$O + O_2 \rightarrow O_3 \tag{1.1}$$

$$O + O_3 \rightarrow O_2 + O_2 \tag{1.2}$$

$$O_3 + hv \rightarrow O_2 + O \tag{1.3}$$

While the (1.1) ~ (1.3) are inadequate to explain the depletion of the ozone in the atmosphere. The reaction with other small components of the atmosphere, X:

$$O + XO \rightarrow X + O_2 \tag{1.4}$$

$$O_3 + X \rightarrow XO + O_2 \tag{1.5}$$

$$O_3 + O \rightarrow O_2 + O_2 \tag{1.6}$$

Where X = OH, NO, ClO, BrO, etc. [9] Before the X is destroyed in other reactions, the molecule X can destroy thousands of ozone molecules. The X abounds in the halogen hydrocarbons which is the major category of the second generation of refrigerants.

The value of ODP (Ozone Depletion Potential) identifies the level of harmfulness to the ozone. The ratio of the impact on ozone of a chemical compared to the impact of a similar mass of R11. Thus, the ODP of R11 is defined to be 1.0. [10]

Therefore, according to the Montreal Protocol on Substances that Deplete the Ozone Layer and Vienna Convention for Protection of the Ozone Layer, the deadline of the utilization of CFCs had been proposed. And the third generation of refrigerants with low ODP value were demanded to gradually replace the second generations. Table 1.3 [4, 6] shows the properties of some most widely used third generation refrigerants with non ODP values.

Table 1.3 The third generation of refrigerants [4, 6]

Refrigerants	Category	Safety	ODP	GWP
R32	HFC	A2L	0	675
R23	HFC	A1	0	14760
R125	HFC	A1	0	3500
R134a	HFC	A1	0	1430
R143a	HFC	A2	0	4470
R152a	HFC	A2	0	124
R404A	HFC	A1	0	3900
R407C	HFC	A1	0	1800
R410A	HFC	A1	0	2100
R507A	HFC	A1	0	4000

1.2.4 The fourth generation

The third generation of refrigerants had successfully controlled the ozone depletion while the new researches and political debate of global warmings become the main problem. GWP is the short name for global warming potential which was firstly introduced in the Inter-governmental Panel on Climate Change (IPCC) [11] and the concept of GWP was further refined [12, 13] to guide and support decisions in industry and environmental policies. From the Table 1.3, almost all the third generation's refrigerants have very large GWP values.

Consequently, United Nations Framework Convention on Climate Change (UNFCCC) had put forward the stipulation: Carbon dioxide (CO_2), methane (CH_4), nitrous oxide (N_2O), HFCs, PFCs and sulfur hexafluoride (SF_6) are the greenhouse gases. And the advanced country should reduce to exhaust greenhouse gases.

Therefore the development of the next generation of refrigerant with low GWP values is extremely urgent. Table 1.4 shows the candidates for the fourth generation of refrigerants. Among all the candidates of next generation of refrigerants, HFOs were recently synthesized as alternatives of HFCs. The researches of the fundamental thermodynamic and kinetic properties are very few. Therefore, the development of new applications using the new low GWP refrigerants is limited by the lack of accurate experimental data.

Table 1.4 The candidates of the fourth generation of refrigerants

Candidates	Considerations
Natural refrigerants	Safety
Low GWP HFCs	Flammability
HCs, HEs	Flammability
HFOs	Flammability, Toxicity, Compatibility

1.2.5 Numbering scheme

The current numbering scheme is based on ASHRAE Standard 34-67 [14] published by American Society of Heating, Refrigerating, and Air conditioning Engineers in 1967. The first character of 'refrigerant'–'R' is the prefix of identifying number of refrigerants and the structure of the molecular is the suffix.

a) Inorganic compounds

The first number of the suffix is '7', so the code of inorganic compounds can be written as R7 + numbers. Within the brackets it is formed by relative molecular mass of compounds.

E.g. Carbon dioxide, CO_2, the relative molecular mass is 44. So the code is R744.

b) Hydrocarbons and derivatives

The molecular formula of the saturated hydrocarbon is C_mH_{m+2}. When the atom of the hydrogen has been replaced by other atoms like fluorine (F), chlorine (Cl), bromine (Br) and others, the formula of the derivatives will be $C_mH_nF_xCl_yBr_z$, and

$$n + x + y + z = 2m + 2 \tag{1.7}$$

The identification number is expressed as R(m-1) (n+1) (x) B (z), if z is 0, the B can be omitted. E.g. Molecular formula: CHF_2Cl, m – 1 = 0, n + 1 = 2, x = 2, z = 0, therefore the identification number is R22.

Molecular formula: CH_4, m – 1 = 0, n + 1 = 5, x = 0, z = 0, therefore the identification number is R50.

However the identification number of n-butane (n-C_4H_{10}) should be R600.

In addition, if the compound is allotropic substance, successive lowercase letters (i.e. a, b or c) are appended. For example, R152a while the iso-butane is R600a.

For cyclic derivatives, the letter 'C' is added at the front of the identification number of the refrigerants. For example, the octafluorocyclobutane (C_4F_8), RC318.

For unsaturated hydrocarbons and its derivatives, the number '1' is added before the refrigerant's identification number. For example, the ethylene (C_2H_3), R1150.

For the fluorinated propene isomers, the numbering scheme is based on the ANSI/ASHRAE Standard 34 [14], agenda adopt nomenclature rules for the ethene (ethylene, R1150, CH_2=CH_2) and propene (propylene, R1270, CH_3CH=CH_2) based refrigerants that have been already implemented in industry and academia. Table 1.5 [15] summarizes those rules that distinguish the propene isomers.

c) Azeotropic and zeotropic mixtures

Azeotropic mixtures is assigned an identifying number in the 500 series. And zeotropic mixtures is assigned an identifying number in the 400 series.

Table 1.5 Proposed suffix scheme for propene isomers [15].

First appended letter		Second appended letter	
Group substitution	Letter	Group substitution	Letter
–Cl	x	$=CCl_2$	a
–F	y	$=CCl_2F$	b
–H	z	$=CF_2$	c
		=CHCl	d
		=CHF	e
		$=CH_2$	f

1.3 Literature review

1.3.1 Thermodynamic properties of R1234ze(Z)

Brown et al. (2009) [16] first provided various estimated thermodynamic properties of R1234ze(Z) by using a cubic equation of state, which are used to predict the performance potential in high temperature heat pumping applications. Also in their work, the theoretical values of critical parameters and acentric factor were presented based on group contribution methods couple with some other estimation techniques. The normal boiling point used in the simulation was taken from Mukhopadhyay et al. (2008) [17]. Brown et al. [16] pointed out R1234ze(Z) deserves further consideration as a substitute for R114.

The experimental data of R1234ze(Z) was firstly published by Kayukawa et al. (2012) [18]. They used Burnett apparatus and metal bellows volumometer to measure the

vapor pressure at temperature from 273 K to 373 K and 310 K to 410 K, respectively. In addition, the experimental data of single phase density for R1234ze(Z) were obtained by these two measurements. The vapor density was measured by Burnett apparatus at temperature from 283 K to 373 K and the metal bellows volumometer was employed for the liquid density from 310 K to 420 K.

Raabe (2012) [19] published evaluated data of vapor pressures and the saturated vapor and liquid densities from 283 K to 373 K that calculated by the Monte Carlo Gibbs ensemble (GEMC) [20].

Fedele et al. (2014) [21, 22] individually measured the vapor pressure data of R1234ze(Z) in two different laboratories, the Istituto per le Tecnologie della Costruzione of the Consiglio Nazionale delle Ricerche (ITC-CNR) and Università Politecnica delle Marche (UnivPM) for the temperature ranging from 283 K to 353 K and 238 K to 372 K, respectively. In addition, the PVT properties were measured in UnivPM for temperatures approximately from 303 K to 375 K and pressures from 0.082 MPa to 0.436 MPa.

Higashi et al. (2015) [23] determined accurate experimental data for the thermodynamic properties of R1234ze(Z). The critical temperature, critical density and critical pressure were measured on the basis of direct observation of the meniscus disappearance [24, 25]. Vapor pressures were measured at temperature region between 310 K and 420 K. Saturated liquid densities and saturated vapor densities were obtained at temperature from 368 K to 422 K and 356 K to 422 K, respectively. The PVT properties cover temperature from 360 K to 432 K and pressure up to 6 MPa for both single liquid and vapor phase, including some data points close to the critical point. The density was calculated from the mass of R1234ze(Z) and the inner volume of pressure cell.

Tanaka (2016) [26] performed measurements for the vapor pressures and saturated liquid density for R1234ze(Z) by using the extraction method in the temperature range from 300 K to 400 K.

All the experimental data available in the literature are summarized in the Table 1.6.

Table 1.6 Summary of experimental data for R1234ze(Z)

Author	Year	Type of data	Reference
Kayukawa et al.	2012	PVT Vapor pressure Vapor and liquid density	[18]
Fedele et al.	2014	Vapor pressure PVT	[21] [22]
Higashi et al.	2015	Critical point Vapor pressure PVT	[23]
Tanaka	2016	Vapor pressure Saturated liquid density	[26]

1.3.2 Thermodynamic properties of R1234yf and the binary mixtures with other refrigerants

Di Nicola et al. (2010) [27] published the vapor pressure data of R1234yf in a temperature range from 224 K to 366 K and at pressures from 0.039 MPa to 3.218 MPa by using a constant-volume apparatus [28]. The data were fitted to the Wagner equation with an absolute deviation of 0.35 %. Tanaka et al. (2010) [29] conducted various measurements of several thermodynamic properties. The critical parameters were determined by the visual observation of the meniscus disappearance [24, 25]. The vapor pressures, saturated liquid density and saturated vapor density were measured by a batch-type calorimeter with a metal-bellows in the temperature range from 310 K to 360 K. Di

Nicola et al. (2010) [30] performed the PVT properties measurement in the vapor phase of R1234yf at temperature from 243 K to 373 K and pressure up to 3.716 MPa. Richter et al. (2011) [31] measured the vapor pressures from 250 K to 366 K. A two-sinker densimeter [32] was applied to determine the PVT properties in the temperature range from 232 K to 400 K and at pressures up to 10 MPa. Fedele et al. (2012) [33] published a total of 13796 compressed liquid density measurements based on a stainless steel vibrating tube densimeter for eight isotherms evenly space from 283.15 K to 353.15 K and for pressures from close to saturation point to 35 MPa. Klomfar et al. (2012) [34] reported the liquid phase PVT properties in the temperature range from 217 K to 353 K with a constant volume apparatus [35] and at pressures from 1 MPa to 40 MPa. Yang et al. (2014) [36] presented vapor pressure measurements for R1234yf at temperature from 248.17 K to 361.05 K. Hu et al. (2017) [37] used single-sinker densimeter [38] to measure the PVT properties in the gaseous phase of R1234yf in the temperature range from 252 K to 345 K and pressures up to 1.91 MPa.

For the binary mixtures of R1234yf and other compounds. Kamiaka et al. (2013) [39] measured vapor-liquid equilibria (VLE) properties for three binary refrigerant mixtures of R1234yf with R32, R125 and R134a at mass fractions of R1234yf from 25 % to 80 %. The equilibrium pressures were obtained at temperatures from 273 K to 333 K at a step of 10 K for each mixture. Akasaka et al. (2013) [40] presented the measurements of saturated densities and critical parameters for binary mixture of R1234yf and R32 near the critical point at mass fraction at mass fraction of R1234yf with 50 %, 80.01 % and 90 %. Hu et al. (2014) [41] reported the VLE properties for binary mixture of R1234yf and R227ea at 10 K intervals from 283.15 K to 323.15 K over whole composition range. Juntarachat et al. (2014) [42] published experimental data for the binary mixture of R1234yf and CO_2 at seven temperatures ranging from 283.15 K to 353.15 K using a static-analytic type apparatus couple with two electromagnetic capillary samplers [43]. Chen et al. (2015) [44] presented VLE properties for binary mixture of R1234yf and R161 over

the whole composition range at temperatures from 283.15 K to 323.15 K at an intervals of 10 K by a recirculation apparatus. Chen et al. (2015) [45] conducted an experiment of PVTx properties in the gas phase for binary mixtures of R1234yf and R134a in the range of temperature from 298.58 K to 403.24 K and pressures from 0.568 MPa to 3.171 MPa. The compositions were mole fraction of R134a from 3.80 % to 86.41 % and the densities varied from 0.258 mol dm^{-3} to 1.258 mol dm^{-3}. Yang et al. (2016) [46] carried out an experiment on the VLE properties for the binary mixture of R1234yf and R245cb system at temperature ranging from 283.15 K to 313.15 K covered all composition range. Higashi (2016) [47] measured various precise thermodynamic properties for the blend of 50 % R1234yf and 50 % R1234ze(E) including PVTx properties from 340 K to 430 K, saturated densities 100 kg m^{-3} to 900 kg m^{-3} and critical parameters. Hu et al. (2017) [48] conducted VLE measurements for binary mixture of R32 + R1234yf and R161 + R1234yf by using a quasi-static analytical apparatus [49] with a whole composition range at the temperature range of 283.15 K to 323.15 K and pressure up to 3.2 MPa and 1.8 MPa , respectively. Cai et al. (2018) [50] measured the single gaseous phase of PVTx properties for blend of R1234yf and R32 by single-sinker magnetic suspension densimeter [38] at temperature from 279.8 K to 347.9 K, pressures from 0.10 MPa to 2.66 MPa and densities from 2.30 kg m^{-3} to 66.02 kg m^{-3}. Mole fractions of R1234yf changed from 0.062 to 0.610.

All the experimental data are summarized in Table 1.7.

Table 1.7 Summary of experimental data for R1234yf and the mixture with other refrigerants

Author	Year	Type of data	Reference
Pure R1234yf			
Di Nicola et al.	2010	Vapor pressure Critical point	[27]
Tanaka et al.	2010	Vapor pressure Saturated liquid and vapor density	[29]
Di Nicola et al.	2010	PVT	[30]
Richter et al.	2011	Vapor pressure PVT	[31]
Fedele et al.	2012	liquid density	[33]
Klomfar et al.	2012	PVT	[34]
Yang et al.	2014	Vapor pressure	[36]
Hu et al.	2017	PVT	[37]
Mixture			
Kamiaka et al.	2013	VLE (R32, R123, R134a)[a] Saturated density	[39]
Akasaka et al.	2013	critical point (R32)[a]	[40]
Hu et al.	2014	VLE (R227)[a]	[41]
Chen et al.	2015	VLE (R161)[a]	[44]
Chen et al.	2015	VLE (R134a)[a]	[45]
Yang et al.	2016	VLE (R245cb)[a]	[46]

Author	Year	Type of data	Reference
Higashi	2016	PVTx Critical point Saturate density (R1234ze(E))[a]	[47]
Hu et al.	2017	VLE (R32, R161)[a]	[48]
Cai et al.	2018	PVTx (R32)[a]	[50]

a. The refrigerants in the bracket are the substances mixed with R1234yf.

1.3.3 Thermodynamic properties of R1123 and the binary mixture with R32.

R1123 is a new refrigerant first manufactured by Japanese refrigerant company [51] which GWP value was estimated within 1. The thermodynamic properties of R1123 and its mixtures are very insufficient. Kayukawa et al. (2015) [52] reported the vapor pressures and PVT properties of R1123 in a wide temperature range. Fukushima et al. (2015) [53] presented the thermodynamic properties of R1123 including the vapor pressures and critical parameters. Higashi et al. (2016) [54] measured PVT properties, vapor pressures, saturated densities and critical parameters. The measurement covered the temperature region from 300 K to 430 K, pressures up to 6.9 MPa and densities between 100 kg m^{-3} and 900 kg m^{-3} along seven isochores. Raabe (2016) [55] used the molecular simulation method to predict thermodynamic properties of R1123 including vapor pressures and saturated densities in the temperature range from 230 K to 300 K. Higashi et al. (2018) [56] conducted saturation pressures measurement for R1123 at temperatures between 278 K and 377 K, and the critical pressures were also obtained.

For the blends of R1123 and other components, Higashi et al. (2016) [54] presented

the PVT properties, VLE properties and critical parameters for the binary mixture of R1123 and R32. The compositions of this mixture were mass fraction of R1123 with 40 % and 60 % and temperature ranges from 310 K to 430 K.

All the experimental data are summarized in Table 1.8.

Table 1.8 Summary of experimental data for R1123 and the mixture with other refrigerants

Author	Year	Type of data	Reference
Pure R1123			
Kayukawa et al.	2015	Vapor pressure	[52]
Fukushima et al.	2015	Vapor pressure Critical point	[53]
Higashi et al.	2016	PVT Vapor pressure Saturated density Critical point	[54]
Higashi et al.	2018	Vapor pressure	[56]
Mixture			
Higashi et al.	2016	VLE Critical point (R32)[a]	[54]

a. The refrigerants in the bracket are the substances mixed with R1123.

1.4 Thesis objective

In the response to the need of developing new low GWP refrigerants, we conducted two kinds of measurements for the PVT and VLE properties. Since some HFOs have insufficient information of thermodynamic properties, the main objective in this study is to provide high accurate data to contribute the development of equation of state.

A Burnett apparatus was modified to perform the PVT measurement for the pure substances in the single gaseous phase at temperature from 353 K to 473 K and pressures up to 10 MPa. The vapor pressure can also be determined if the initial state inside sample cell is vapor liquid equilibrium condition. To verify the apparatus at first step, some samples with known published data and existing EOS should be measured to test the reliability. The refrigerants utilized in the PVT measurements are the candidates for those used in the high temperature heating pump system.

For the measurement on VLE properties of binary mixtures, the apparatus was designed for the temperature region between 253 K and 423 K. The composition was determined by a gas chromatograph. First the conversion factors that transfer the area ratio of each peaks to concentrations were calculated by measuring the target samples with known mass fraction. Then target samples were measured and the results were compared with existing data and EOS to verify the reliability of the apparatus and needed for the determination of the mixing parameters in mixing models.

The scopes of the present work are as follows:

(1) The apparatus of PVT and VLE properties measurements are designed to provide accurate data for developing accurate EOS. PVT measurements were conducted at high temperature region and VLE measurements were for the low temperature systems.

(2) Helium, nitrogen and R134a were measured by Burnett apparatus to verify the reliability. The densities of each compounds were calculated and discussed.

(3) The conversion functions of gas chromatograph were determined by measuring the binary mixtures of R32+R1123, R32+R1234yf and R1123+R1234yf at room temperature.

(4) R1234ze(Z) was measured by Burnett method at temperature from 353 K to 413 K at an interval of 20 K.

(5) Binary mixture systems of R32, R1123 and R1234yf were measured to determine the VLE properties at temperature from 273 K to 313 K at a step of 10 K.

1.5 Thesis outline

The following is the brief description of the contents of each chapter.

Chapter 1 presents the scientific background and literature review about the thermodynamic properties of HFOs in this study. The vapor pressures, saturated liquid densities, saturated vapor densities, critical parameters and PVT properties are described. The historical development of refrigerants are also introduced and numerical scheme is presented.

Chapter 2 presents the details of the Burnett apparatus and briefly introduced the Burnett method. The temperature measurement by standard platinum resistance thermometer (SPRT) and pressure measurement by absolute pressure transducer are

discussed. The basic mathematical analysis is introduced for the calculation of densities and determination of compressibility factors. The experimental procedure and special supply system are described. The uncertainties of the experiments are analyzed.

Chapter 3 presents the details of the apparatus for VLE measurement. The temperature and pressure measurements are described and the composition measurement is introduced. Experimental procedure is carefully described. The uncertainties of the experiment are analyzed.

Chapter 4 presents the experimental results from Burnett method. The data of PVT properties of Helium, nitrogen and R134a are introduced and compared with existing EOSs. The deviations of the density and pressure are given. The results of R1234ze(Z) are discussed and compared with other published data and the EOSs. The distribution of the existing data are described.

Chapter 5 presents experimental results for VLE properties. The conversion factors for the composition measurement are introduced. The data of binary blend of R32 + R1234yf is compared with Kamiaka et al.'s data and the existing EOS. Deviations of bubble and dew point pressure are given. The data of binary mixtures of R32 + R1123 and R11234 + R1234yf are discussed and compared with mixing model. The data are correlated with the Peng-Robinson equation.

Chapter 6 presents the overall conclusion of this thesis.

Chapter 2 Burnett Method

In this chapter, the principle, apparatus and experiment processes of Burnett method are introduced in the following subsections. The fundamental equations are shown and pictures of the experimental devices are attached. The experimental procedure are described in details and a supplying method is introduced.

2.1 Introduction

To acquire more accurate PVT properties data at high temperatures and high pressures, E.S. Burnett (1936) [57] invented a method for determining compressibility factors without directly measuring volume or mass. The schematic diagram of the Burnett method is show in Fig. 2.1.

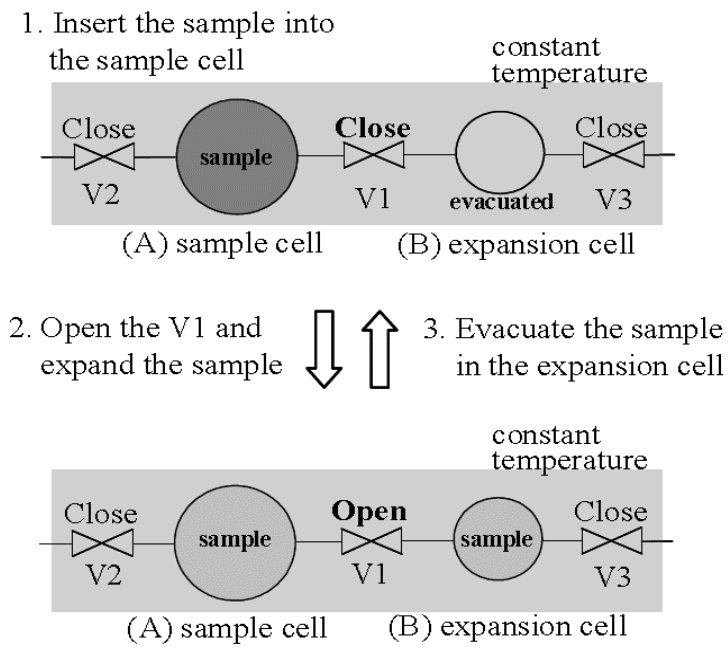

Figure 2.1 The schematic diagram of the Burnett method.

Two vessels are installed, one is called the sample cell and another is called the expansion cell. Firstly, the substance is filled in the sample cell and then expanded into the evacuated expansion cell repeatedly. After several expansions, the state of the substance remains in the system can be considered as the ideal gas which means the fundamental equation of state of the ideal gas can be applied into calculating the PVT properties. The densities at each state are evaluated by measuring the equilibrium pressures before and after the expansions. The advantage of this method is that mass measurement is not necessary, so that makes this method one of the most effective measurements for PVT properties for the gas phase region.

2.2 Fundamental equations

The PVT relation of the sample in the system can be expressed by the following equation with the compressibility factor, Z

$$PV = ZmRT \tag{2.1}$$

Where P is the pressure, T is the temperature, R is the gas constant, V is the volume, m is the mass of the substance. The subscript *i* denotes the times of expansions, therefor, for i^{th} expansion at constant temperature, the PVT relation of the sample in the sample cell is expressed by

$$P_{i-1}V_A = Z_{i-1}mRT \tag{2.2}$$

The PVT relation after expansion is expressed by

$$P_i(V_A + V_B) = Z_i mRT \tag{2.3}$$

Where V_A is the volume of sample cell and V_B is the volume of the expansion cell. When $i = 1$, P_0 denotes the initial pressure and Z_0 denotes the initial compressibility of the sample before the first expansion. Dividing Eq. 2.3 by Eq. 2.1 gives

$$\frac{P_i(V_A+V_B)}{P_{i-1}V_A} = \frac{Z_i}{Z_{i-1}} \tag{2.4}$$

Here, with the definition of volume ratio $N = (V_A + V_B)/V_A$, which is also called

the cell constant determined by the sample and expansion cells. Eq. 2.4 gives

$$\frac{P_i}{P_{i-1}}N = \frac{Z_i}{Z_{i-1}} \tag{2.5}$$

After infinite times of expansions, the cell constant is expressed by

$$N = \lim_{i\to\infty}\frac{Z_i}{Z_{i-1}}\frac{P_{i-1}}{P_i} = \lim_{i\to\infty}\frac{P_{i-1}}{P_i} \tag{2.6}$$

From Eq. 2.5,

$$\prod_{i=1}^{n}\left[\frac{P_i}{P_{i-1}}N\right] = \prod_{i=1}^{n}\left[\frac{Z_i}{Z_{i-1}}\right] \tag{2.7}$$

is obtained and rewritten as

$$\frac{P_n}{P_0}N^n = \frac{Z_n}{Z_0} \tag{2.8}$$

After expanding the sample infinitely, it is considered as the ideal gas state, the compressibility factor,$Z_n = 1$ and the initial compressibility factor Z_0 is determined by

$$\lim_{n\to\infty}\left(\frac{P_n}{P_0}N^n\right) = \frac{1}{Z_0} \tag{2.9}$$

Thus, for each expansion the compressibility factor Z_n is calculated from

$$Z_n = Z_0(\frac{P_n}{P_0}N^n) \tag{2.10}$$

According to the definition of the compressibility factor, the density of the sample ρ_n is calculated by

$$\rho_n = \frac{P_n}{Z_n RT} \tag{2.11}$$

In practice, infinite expansion is not reachable. To obtain the value of the volume ratio from the Eq. 2.6, a polynomial equation, which independent variable is P_i and dependent variable is P_{i-1}/P_i, is developed to determine the N as the intercept of the equation.

2.3 Experimental apparatus

2.3.1 Schematic diagram of the experimental devices

The schematic diagram of the apparatus of the Burnett method is shown in the Fig.

2.2. This apparatus was originally designed for the PVT measurement of hydrogen [58]. In this research, a modification was conducted to adjust the apparatus for the measurement of refrigerants. The device of pressure measurement for the sample is an absolute pressure transducer (Paroscientific Co. Ltd. Model 42K-101, maximum pressure region is 13.8 MPa). Isothermal oil bath with the heat transfer media of silicone oil is utilized, and the temperature of the oil bath is measured by a standard platinum resistance thermometers (SPRT, NETSUSHIN Co. Ltd. Model NSR – 660) and a precise thermometer AC bridge (ASL Co. Ltd. Model F700B) according to the International Temperature Scale 1990 (ITS90).

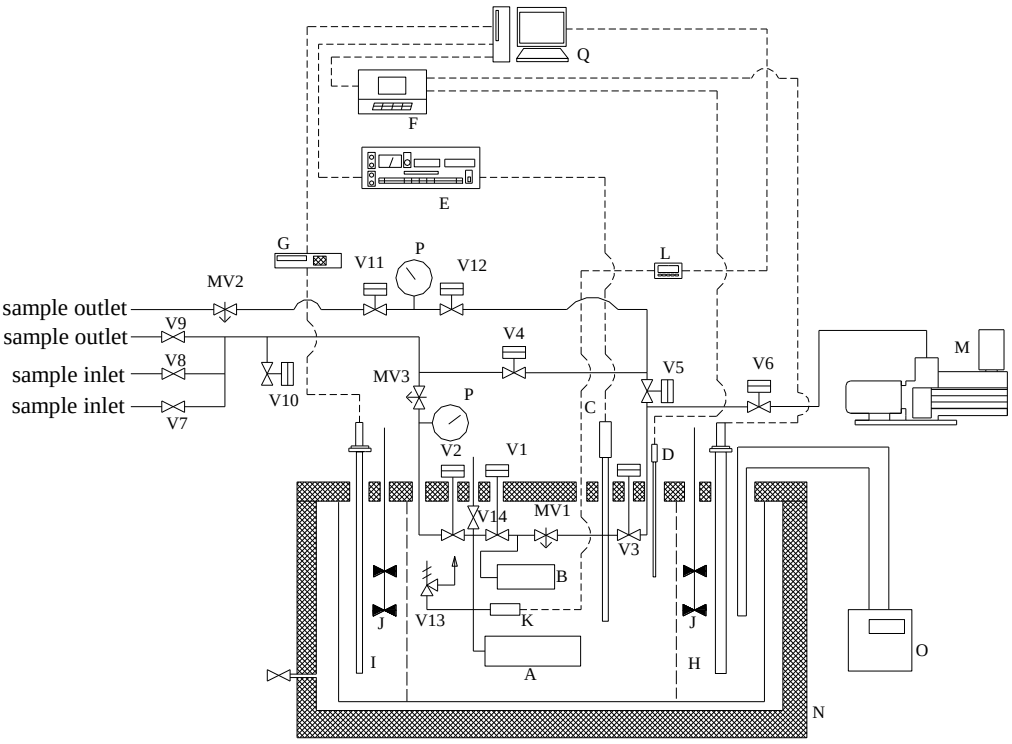

A: sample cell B: expansion cell C: platinum resistance thermometer D: thermometer
E: thermometer bridge F: temperature controller G: DC power supply H: main heater
I: subheater J: stirrer K: quartz pressure transducer L: digital pressure indicator
M: vacuum pump N: constant temperature bath O: circulation bath P: pressure gauge
Q: personal computer V1～V14, MV1～3: valves

Figure 2.2 The schematic diagram of the apparatus.

2.3.2 Pressure vessels

Two cylindrical pressure vessels are installed, one is the sample cell and another is the expansion cell. The inner volumes of the two cells are 250 cm^3 and 100 cm^3, respectively. The maximum designed temperature and pressure of the two vessels are 523 K and 100 MPa. The inner and external diameters of the two cells are the same, 35mm and 85 mm. Thus the only difference between the two cells are the length, the length of sample cell is 412 mm and the length of the expansion cell is 256 mm. To make the cells smaller, the Inconel alloy 625 is used because of the larger strength compared with stainless steels at high temperatures.

2.3.3 Isothermal bath and SPRT

Since the experimental condition is isothermal, the constant temperature bath is required. The sample and expansion cell are immersed in the silicon oil for the isothermal expansions. The silicon oil is constantly stirred by four motors (Oriental motor Co. Ltd. Model 5IK40A-SYN, 40 W) to increase or maintain the temperature.

The temperature of the oil bath is measured by the standard platinum resistance thermometer (SPRT), the specification is shown in the Table 2.1. At the vertical direction, the SPRT is installed which is connected with the precision AC bridge (ASL model F700B). The Model F700B is a high accuracy resistance bridge designed specifically for use in resistance thermometry. Its unique AC bridge circuitry eliminates thermal EMF effects to provide fast, reliable measurements under a wide range of real operating conditions, the specification of the F700B is shown in the Table 2.2.

Table 2.1 Specification of the SPRT

Model	NSR 660
Resistance at 273.15 K	25 Ω
Specified Current	1 mA
Resistance Ratio	R(Ga)/R(0.01) ≥ 1.11807
Temperature Region	273 K ~ 933 K
Basic Accuracy	± 0.001 K
Sensitivity	0.1 Ω/K
Insulation Resistance	DC 100V/100 MΩ
Texture of the Protective Tube	SUS316
Diameter of the Protective Tube	Φ 6.0 mm
Length of the Protective Tube	600 mm

Table 2.2 Specification of F700B

Accuracy	± 0.25 mK
Resolution	0.25 mK
Linearity	± 0.25 mK
Warm up time	< 30 seconds

According to the ITS90 [59], the relationship between the resistance ratio of the standard platinum resistance thermometer and the triple point of the water is expressed by:

$$\mathrm{W}(T_{90}) = \frac{R(T_{90})}{R(273.16\ \mathrm{K})} \tag{2.12}$$

Where R (273.16 K) is resistance of SPRT at the triple point of water, T_{90} refers to the temperature on ITS-90.

The deviation of the SPRT can be expressed by the following interpolated equation,

$$W_r(T_{90}) = W(T_{90}) - \Delta W(T_{90}) \tag{2.13}$$

$W_r(T_{90})$ is a correction to $W(T_{90})$. $\Delta W(T_{90})$, called the deviation function for the SPRT, depends on the temperature range and can be determined during calibration. In this experiment, the deviation function is expressed as,

$$\Delta W(T_{90}) = a(W(T_{90}) - 1) + b(W(T_{90}) - 1)^2 + c(W(T_{90}) - 1)^3 \tag{2.14}$$

Here a, b and c are the adjustable parameters which are the calibration constants for the SPRT. Once the value of $W_r(T_{90})$ has been determined, the temperature can be calculated. For the temperature region above 273.16 K, the reference function can be expressed as:

$$T_{90} - 273.15 = D_0 + \sum_{i=1}^{9} D_i \left[\frac{W_r(T_{90}) - 2.64}{1.64}\right]^i \tag{2.15}$$

The constants of the formula are given in the Table 2.3.

Table 2.3 Constants

D_0	439.932854	D_5	0.005184
D_1	472.418020	D_6	- 0.963864
D_2	37.684494	D_7	- 0.188732
D_3	7.472018	D_8	0.191203
D_4	2.920828	D_9	0.049025

2.3.4 Modification of the pressure transducer

The pressure transducer was firstly installed on the top of the apparatus as shown in the Fig. 2.3 (a). However, during the measurement of refrigerants, the pressure was difficult to get to stable state and large deviation was observed. The main reason was the effect from the dead space between the pressure transducer and the cells. Therefore, a modification was conducted as shown in the Fig 2.3 (b). The pressure transducer was immersed in the thermostat bath close to the sample cell at the same horizontal position. After this modification, the effect of the dead space was eliminated.

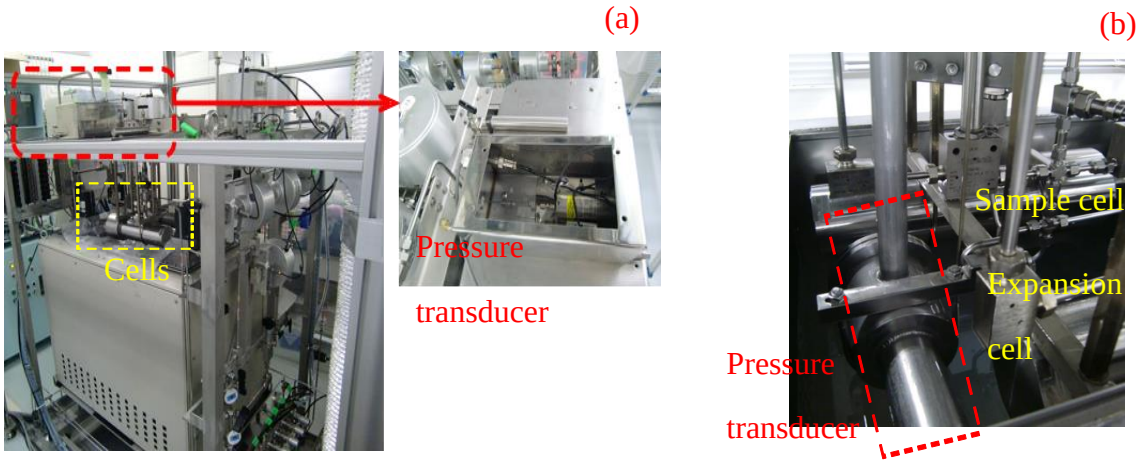

Figure 2.3 (a) The initial position of pressure transducer (b) modification of the pressure transducer.

2.4 Experimental procedure

2.4.1 Steps of measurement

The first step of this experiment is to turn on the vacuum pump to evacuate both the sample cell and expansion cell before supplying the objective substance.

Fig. 2.4 shows the operation panel to control the system. Opening the valve V2 and closing V1 by clicking the icon, the sample will flow into the sample cell. After waiting for several minutes until the pressure is stable, all the opened valves should be closed, release the sample that remains in the pipe and evacuate it. Then the temperature of the oil bath will be increased to the target temperature. Waiting for several minutes until the pressure is stable, the times of expanding should be estimated based on the initial pressure at the each temperature.

Opening V1, the sample expands into the expansion cell, and then V1 closes waiting for the pressure become stable. Afterwards, evacuating the expansion cell to prepare for the next expansion. All the data of the pressure and temperature is recorded automatically by the Labview that is saved as the profile of txt type. Repeating this process as many as

estimated times.

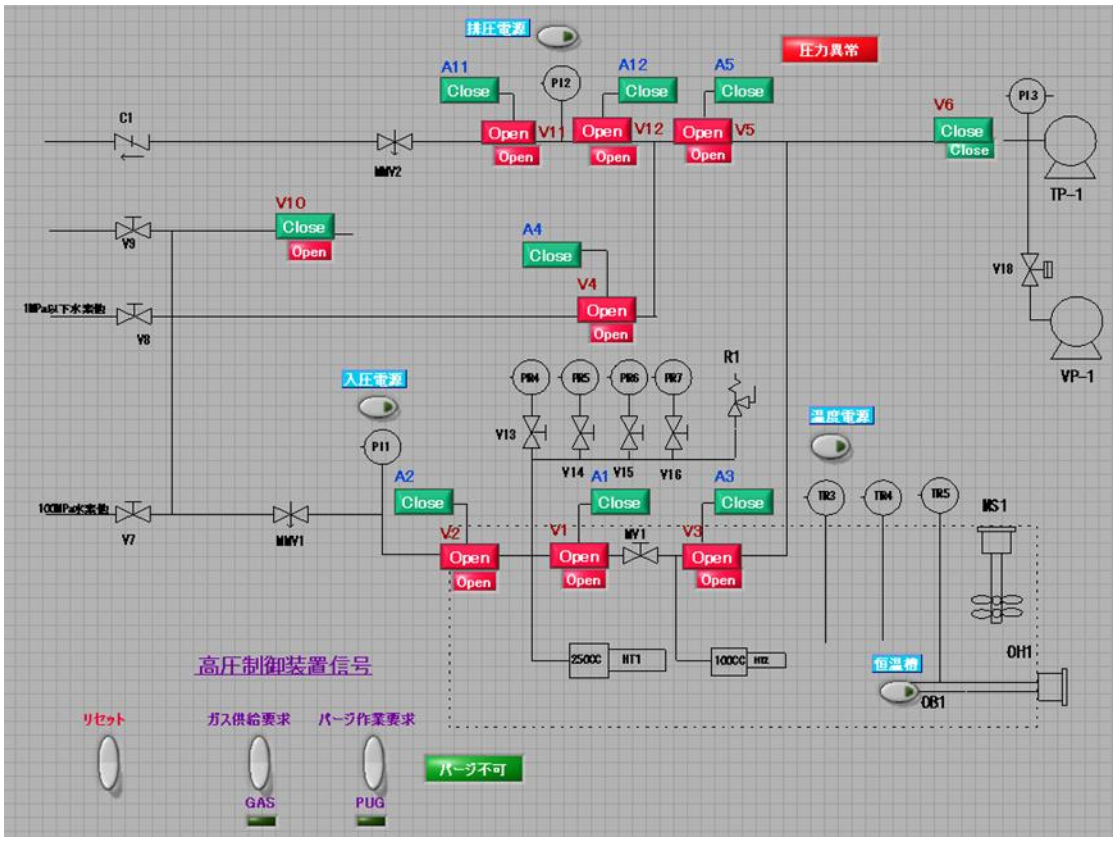

Figure 2.4 The operation panel of the control system

2.4.2 Supplying method for R1234ze(Z)

The sample of R1234ze(Z) is stored in a cylinder at room temperature (297 K) and at saturated vapor pressure up to 0.17 MPa in vapor-liquid phases. In this experiment, there is no pressure pump installed. Therefore when the sample is filled into the sample cell at room temperature, the maximum pressure that we can achieve inside the cell is limited by 0.17 MPa. After the temperature was increased, the pressure inside the cell decrease to an extremely low value. Limited by the accuracy of the absolute pressure

transducer, the data obtained at the extremely low region is not accurate enough that uncertainty of the experiment shall become too much.

Therefore, a new procedure is developed. The schematic diagram of this supplying method is shown in the Fig. 2.5.

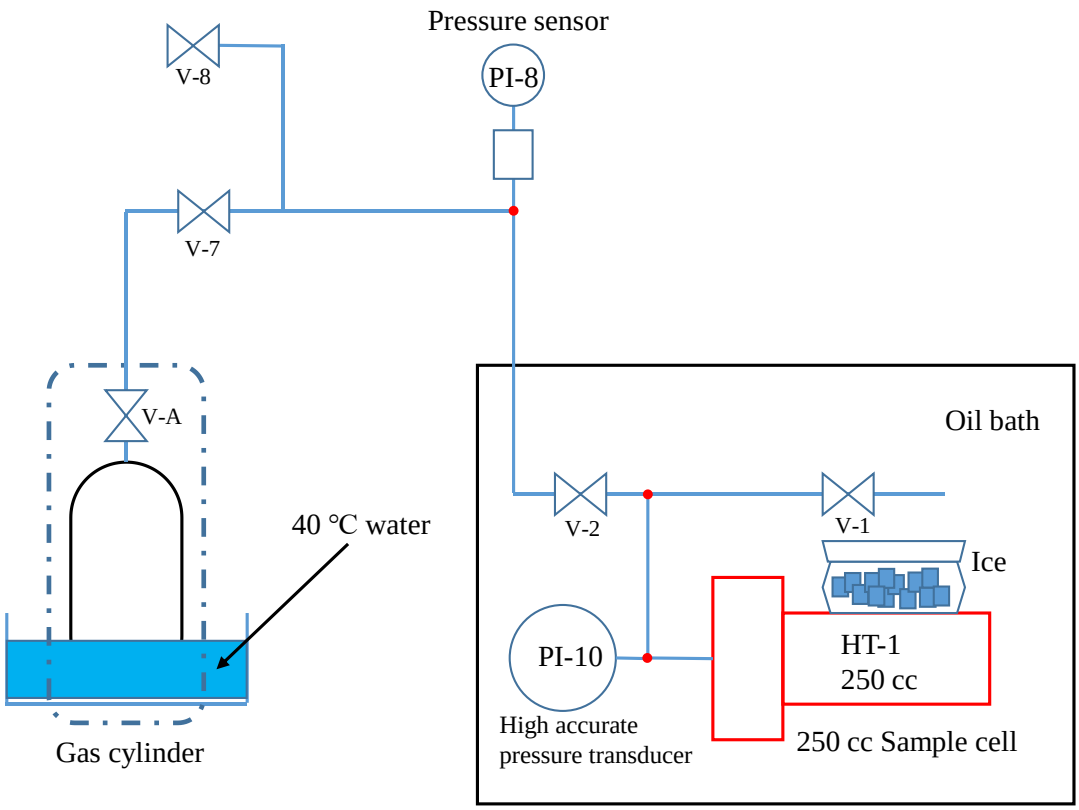

Figure 2.5 The schematic diagram of supplying method

The gas cylinder of the R1234ze(Z) is placed in a tray. The pressure sensor PI-8 is used to monitor the pressure in the pipe. V-A, V-1 and V-8 are closed, V-7 and V-2 are open at the initial state. The procedure is described as follows.

(1) The valve V-A is opened to fill the sample into the sample cell (HT-1, 250cc) at room temperature (297 K) and at pressure up to saturated vapor pressure (0.17 MPa).

(2) V-2 closed and 313 K water is filled into the tray to increase the temperature of sample inside the cylinder. The pressure rises to 0.3 MPa which is the saturated vapor pressure at 313 K.

(3) Some plastic bags full with ice are placed upon the external surface of the sample cell to decrease the temperature inside.

(4) Closing V-A and opening V-2, the sample in the pipe flows into the sample cell and wait for several minutes until the pressure is stable.

(5) Closing V-2 and opening V-A the sample of high pressure inside the cylinder flows into the pipe.

(6) Repeat step 4 and 5 several times until the objective pressure is achieved.

(7) V-A and V-2 are closed, V-8 opens to release the gas remains in the pipe and then replace the gas cylinder.

2.5 Uncertainties of experimental data

The uncertainty of temperature measurement is evaluated to be within 6 mK and for the pressure measurement the uncertainty is estimated to be within 0.3 kPa. In this study, the coverage factor k is chosen to be $k = 2$ [60]. Therefore the uncertainty of density was expressed as [61]:

$$\frac{u(\rho_i)}{\rho_i} = \left[\left(\frac{u(\rho_m)}{\rho_m} \right)^2 + (m-i)^2 \left(\frac{u(N)}{N} \right)^2 \right]^{1/2} \tag{2.15}$$

Where ρ is the density and subscripts i and m denote the times of expansion, respectively. $u(N)$ presents the uncertainty in the cell constant [58]. In this study, the uncertainties are lowest at final expansion and highest at initial state and estimated to be 0.05 % and 0.12 %.

Chapter 3 Vapor-Liquid Equilibrium Measurement

In this chapter, the details of the apparatus and experimental procedure are introduced. The correlation for composition measurement has been determined. The uncertainties are discussed.

3.1 Experimental apparatus

3.1.1 Outline of the experimental facilities

A schematic diagram of the apparatus is shown in Fig. 3.1. The apparatus has been developed from previous work [62, 63] and consists of a thermostated bath, an equilibrium cell, two cells for vapor and liquid side, and some measuring devices. The inner dimensions of the bath are length 640 mm × width 400 mm × height 470 mm and 5 mm for the wall thickness except the top wall. The equilibrium cell is immersed in the thermostated bath and its temperature was controlled by means of an electric subheater and a cooling pump. Two stirrers are utilized to flow the medium inside the thermostat bath and ensure the uniform distribution of temperature. Silicon oil (Shinetsu, KF-96-20CS) of low viscosity due to low experimental temperature region was used as the heat transfer medium. The sample filled in the equilibrium cell in the vapor-liquid equilibrium state and isothermally extracted to the vapor-side and liquid-side cells through the hexagon valves, respectively. The sample temperature was detected by a standard platinum resistance thermometer (Netsushin, NSR-LT40) placed on the equilibrium cell wall with a precise thermometer bridge (ASL, F650). The sample pressure was measured by a quartz pressure transducer (Paroscientific, 42K-101) located inside the thermostated bath.

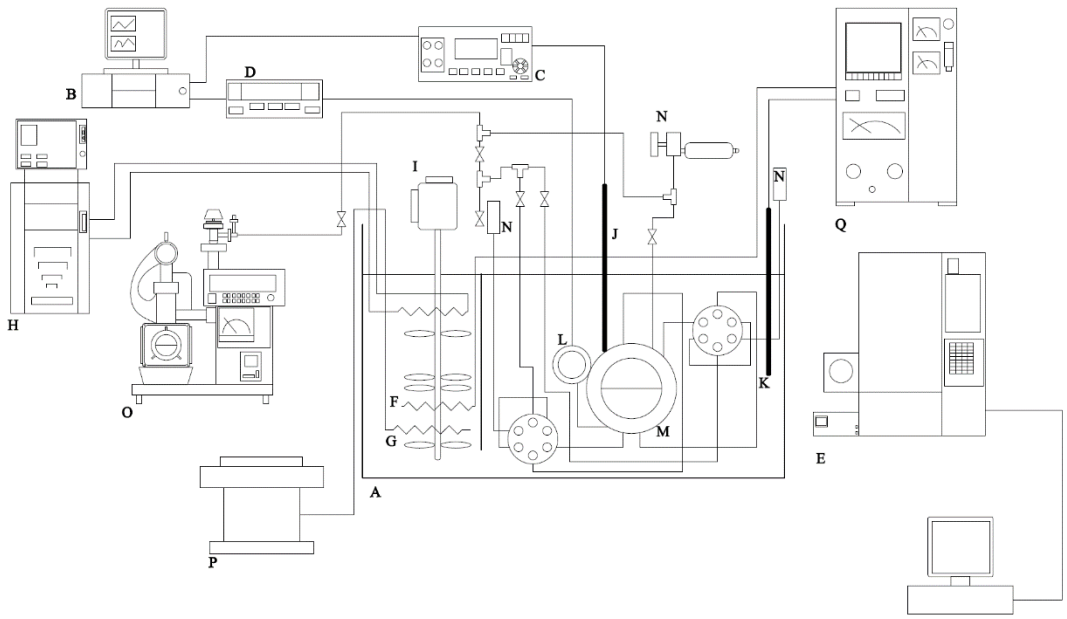

Figure 3.1 Schematic diagram of the VLE property measurement apparatus: A, Liquid bath; B, R, personal computer; C, thermometer Bridge; D, pressure computer; E, gas chromatograph; F, G, electric heaters; H, cooling pump; I, stirrer; J, standard platinum resistance thermometer; K, hexagon valve; L, pressure transducer; M, equilibrium cell; N, sample vessel; O, vacuum pump; P, power supply; Q, PID controller.

3.1.2 Structure inside the thermostat bath

As shown in the Fig 3.2 (a), the equilibrium cell with an inner volume of 163 cm^3 was directly connected to two hexagon valves, circulation pumps, pressure transducer and a vapor-side expansion vessel. The sample was supplied into the cell from top in liquid-vapor equilibrium phase condition. At the front and back of the cell, two glasses installed through which one can observe the phase change as shown in the Fig. 3.2 (b). All of these devices are immersed into the thermostat bath to eliminate the influence of condensation.

(a)

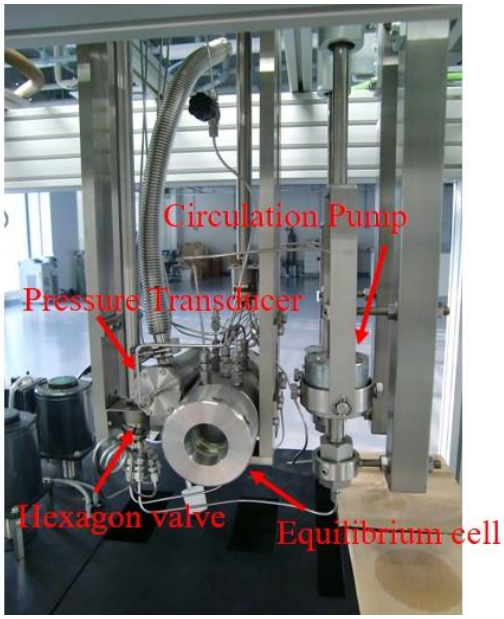

(b)

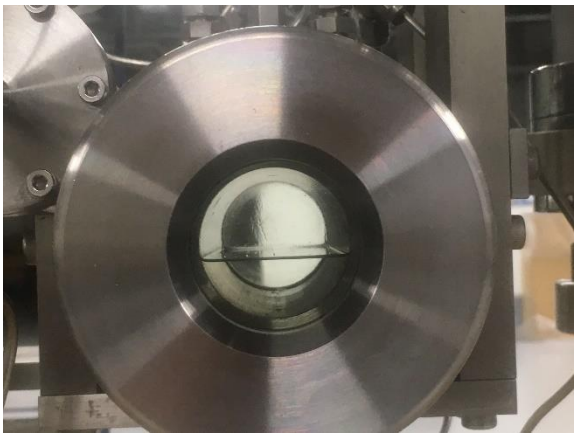

Figure 3.2 The pictures of the equilibrium cell; (a), main system of the VEL apparatus; (b), the equilibrium cell with sample inside.

3.1.3 Temperature control system

The target experimental temperature region is from 253 K to 323 K. Consequently, a liquid-cooling system was applied. As shown in the Fig. 3.1, the cooling pump (Julabo, F32-HE) is connected to the thermostat bath and value of the cooling pump was set 10 K lower than the target temperature as a basement temperature. A main heater and a subheater are installed to increase the temperature. The PID controller (CHINO, SU) is applied to control the temperature of the thermostat bath.

3.1.4 Temperature measurement

A standard platinum resistant thermometer (NSR-LT40) is installed at the outer surface of the equilibrium cell and connected with a precision AC bridge. The specifications of the SPRT and bridge are shown in the Table 3.1 and 3.2.

Table 3.1 Specification of the SPRT

Model	NSR-LT40
Resistance at 273 K	100 Ω
Specified Current	1 mA
Resistance Ratio	R(Ga)/R(0.01) ≥ 1.11807
Temperature Region	233 k~ 433 K
Basic Accuracy	± 0.003 K
Sensitivity	0.4 Ω/K
Insulation Resistance	DC 100V/100 MΩ
Texture of the Protective Tube	SUS316
Diameter of the Protective Tube	Φ 4.8 mm & Φ 6.0 mm
Length of the Protective Tube	600 mm

Table 3.2 Specification of F650

Accuracy	± 0.25 mK
Resolution	0.25 mK
Linearity	± 0.25 mK
Warm up time	< 30 seconds

The details of calibration method for the temperature measurement was described in chapter 2 for the SPRT.

3.1.5 Extraction system

Two cells are prepared, one is for the vapor side with an inner volume of 25 cm^3 and another is for the liquid side with an inner volume of 50 cm^3.There are two hexagon valves installed among the paths for both vapor and liquid sides. The working principle is shown in the Fig. 3.3, the flowing direction will be changed by turn handle. For the vapor side, among path 1 and 5 there is an expansion cell and for the liquid side, between path 1 and 5 there is a coil pipe. The paths 2 and 3 are directly connected with the sample cell at liquid and vapor side, respectively. The path 4 connects to the gas chromatograph. The position A is the initial state when no expansion conducted, and when the position turns to B, the sample will be extracted to the coil pipe in liquid phase and vapor-side cell in vapor phase simultaneously. Then turn the vales back to position A, the sample in the coil pipe expanded to liquid-side cell and become single gaseous phase. At this time, sample can be supplied to the gas chromatograph and the compositions in the liquid and vapor side can be determined.

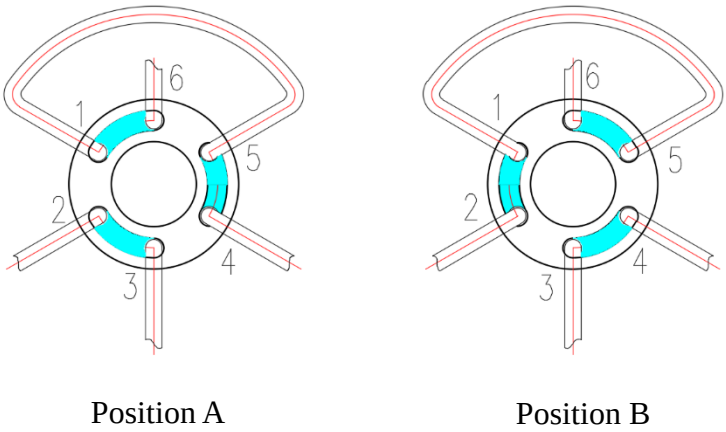

Figure 3.3 The schematic diagram for the working principle of hexagon valves.

3.1.6 Gas chromatograph

The composition of substances are measured by a gas chromatograph (GC-2014) manufactured by Shimadzu co. Ltd. The inlet connected to the VLE apparatus is covered by an air-controlled valve. It is operated automatically by applying nitrogen. The sample of gaseous compounds is adhered to the inside of a solid matrix inside a large metal tube (a packed column) and analyzed. In this study, the detection of thermal conductivity is utilized with the carrier gas of helium. The results obtained from gas chromatograph are in the peaks diagram and the appearing time and area of each peak can also be recorded as shown in the Fig 3.4. However the area ratio of each peak can't represent the concentration directly. To calculate the composition, the correlation between the area ratio and concentration should be determined by measuring standard mixtures with known concentration. In this study, the standard binary mixtures are made by measuring the weight before and after supplying the components into a sample cell. An electronic balance precisely weighed to 0.1 mg was used. The correlations of the target mixtures are

determined and the details are described below.

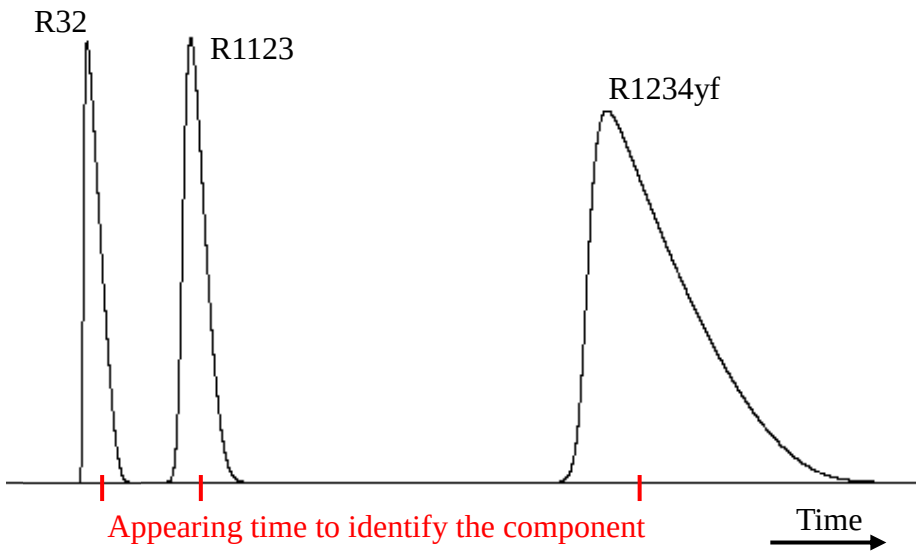

Figure 3.4 The schematic diagram of the results from gas chromatograph

3.2 Correlation between the area ratio and concentration

3.2.1 R32 + R1123

The mass concentration of R1123 the binary mixtures in gaseous phase were weighed to be 39.52 % and 59.96 %, respectively. Standard samples were supplied to the gas chromatograph and the results are summarized in the Table 3.3. By applying the molar mass of R32 and R1123, the mole fraction can be calculated and presented in the Table 3.3. As shown in the Fig. 3.5, the conversion functions have been determined by analysis of polynomial fitting. The functions are expressed as:

$$y_{mass} = -0.0024x^2 + 1.2375x + 0.0268 \quad (3.1)$$

Where y denotes the concentration, x is the area ratio of R1123 obtained from gas chromatograph.

Table 3.3 Results from gas chromatograph for binary mixture R32 + R1123

Area ratio of R1123	Mass fraction of R1123
34.455	39.952
54.152	59.96

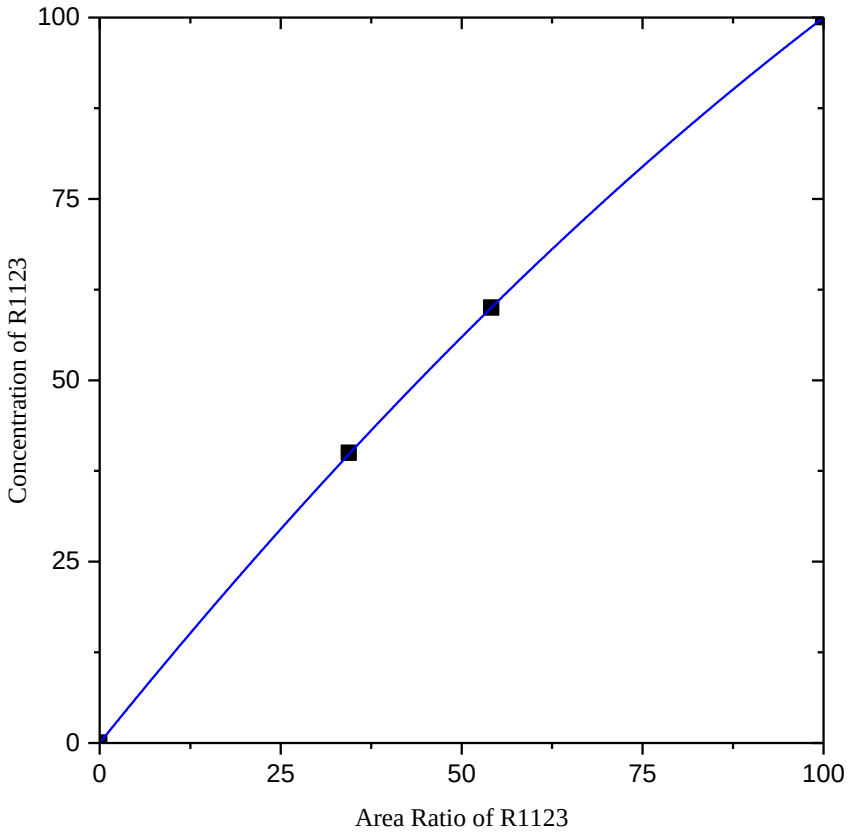

Figure 3.5 The correlation curve of area ratio and concentration for R32 + R1123

3.2.2 R32 + R1234yf

Procedures are the same as R32 + R1123. The mass fraction of R1234yf of standard mixtures are 50 % and 80 %. Results are shown in Table 3.4 and Fig. 3.6. The functions are expressed as:

$$y_{mass} = -0.0034x^2 + 1.3398x + 0.0694 \tag{3.2}$$

Where *x* denotes the area ratio of R1234yf in this mixture.

Table 3.4 Results from gas chromatograph for binary mixture R32 + R1234yf

Area ratio of R1234yf	Mass fraction of R1234yf
41.542	50.100
73.879	80.052

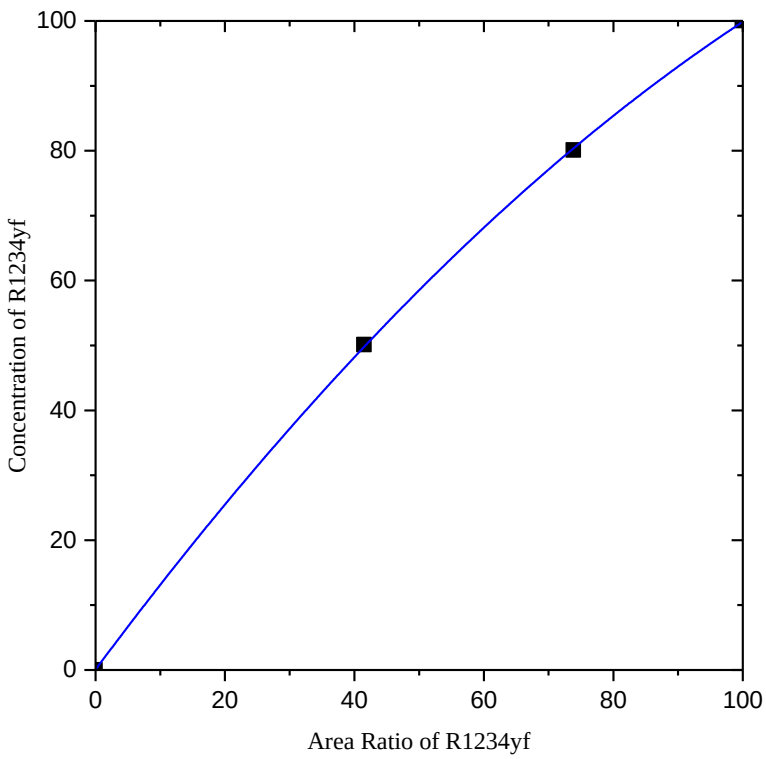

Figure 3.6 The correlation curve of area ratio and concentration for R32 + R1234yf

3.2.3 R1123 + R1234yf

The mass fractions of R1234yf are 70.079 % and 24.903%. Results are shown in Table 3.5 and Fig. 3.7. The functions are expressed as:

The functions are expressed as:

$$y_{mass} = -0.0011x^2 + 1.1092x - 0.0218 \tag{3.3}$$

Table 3.5 Results from gas chromatograph for binary mixture R1123 + R1234yf

Area ratio of R1234yf	Mass fraction of R1234yf
23.033	24.903
67.663	70.079

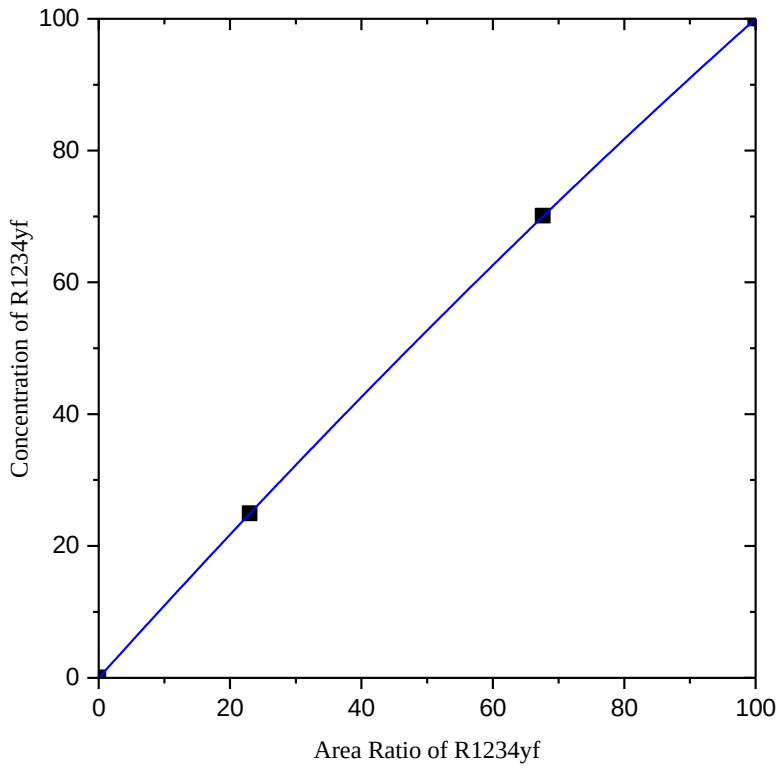

Figure 3.7 The correlation curve of area ratio and concentration for R1123 + R1234yf.

3.4 Uncertainties

The uncertainties of the measurements are analyzed. In this study the coverage factor *k* is chosen to be *k* = 2. The uncertainties of the temperature and pressure measurement are estimated to be 9 mK and 1.38 kPa, respectively. And the relative uncertainty of the calibration curve is about 0.1 % in mass fraction and 0.12 % in the repeatability. The relative uncertainty of the composition measurement is estimated to be 0.15 %.

Chapter 4 Experimental Results on PVT Properties

In this chapter, the experimental PVT data of helium (He), nitrogen (N_2) and 1,1,1,2-tetrafluoroethane (R134a) are described and compared with the existing EOSs to verify the reliability of the new modified apparatus. Twenty-nine PVT properties data of target refrigerant cis-1,3,3,3-tetrafluoropropene (R1234ze(Z)) are obtained and compared with other experimental data and EOS. The information of the sample used in this measurement is given in the Table 4.1.

Table 4.1 Sample Information

Sample	Purity	Manufacture
Helium	99.995%	Japan Helium Center Co., Ltd.
Nitrogen	99.995%	Fukuoka Oxygen Co., Ltd.
R134a	99.98%	Daikin Industries, Ltd.
R1234ze(Z)	99.96%	Central Glass Co., Ltd.

4.1 PVT property measurements for helium

4.1.1 Experimental results

Helium was filled into the sample cell and the temperatures of the oil bath were heated up to 353 K, 373 K, 393 K and 413 K, respectively. At each temperature, the initial pressures before expansion were 1.13 MPa, 1.14 MPa, 1.19 MPa and 1.25 MPa, respectively. Considering the feature of Burnett Method, five times of expansion were conducted and the pressures before and after the expansion were obtained as shown in the Fig. 4.1. Thus, the pressure ratio can be determined based on the experimental data and according to Eq. 2.6 the cell constant will also be calculated. The subscript i denotes the times of expansions and therefore the vertical axis is the pressure ratio before and after i^{th} expansion. In this study the cell constant is N = 1.39760 ± 0.00005 regardless of the temperature dependence as shown in the Fig 4.2. From the Eq. 2.9, the initial compressibility factors of each temperature are calculated as shown in the Fig. 4.3. With the compressibility factors of each state, the densities of helium were evaluated.

The experimental results are summarized in the Table 4.2.

Table 4.2 Experimental results of PVT properties for helium from 353 K to 413 K

Pressure (MPa)	Density (mol dm^{-3})
T / K=353.163	
1.1312	0.3835
0.8084	0.2744
0.5779	0.1964
0.4132	0.1405
0.2955	0.1005
0.2114	0.07193
T / K=373.167	
1.1437	0.3671
0.8174	0.2627
0.5843	0.1879
0.4179	0.1345
0.2988	0.09621
0.2138	0.06884
T / K=393.119	
1.1969	0.3647
0.8554	0.2609
0.6115	0.1867
0.4373	0.1336
0.3127	0.09557
0.2237	0.06838
T / K=413.134	
1.2495	0.3623
0.8930	0.2592
0.6385	0.1855
0.4566	0.1327
0.3265	0.09496
0.2336	0.06795

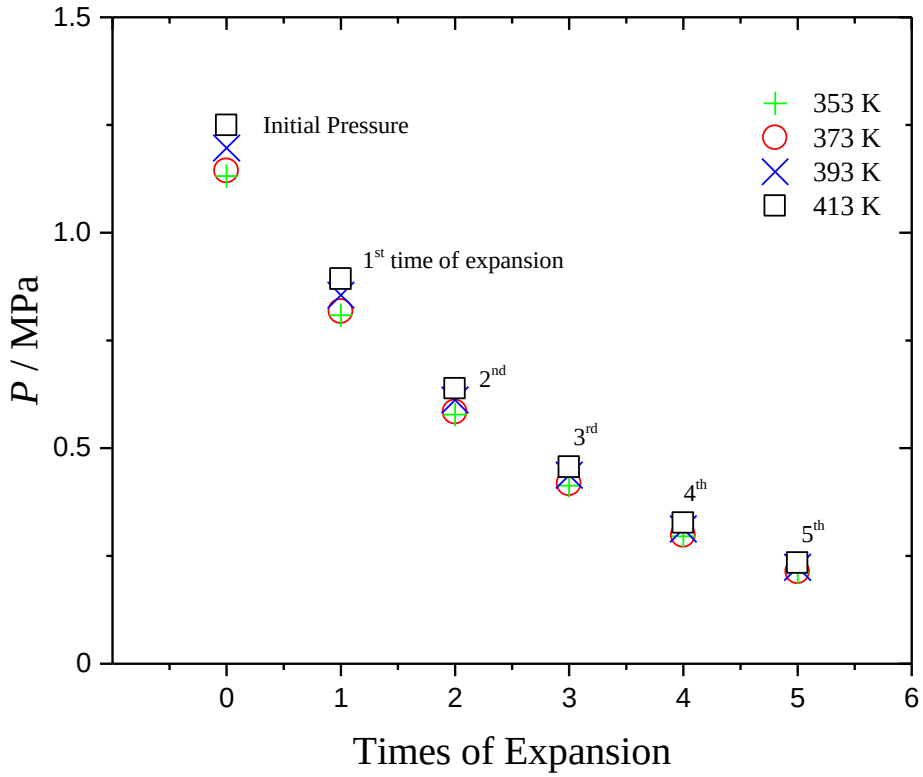

Figure 4.1 Pressures of helium after each expansion from 353 K to 413 K

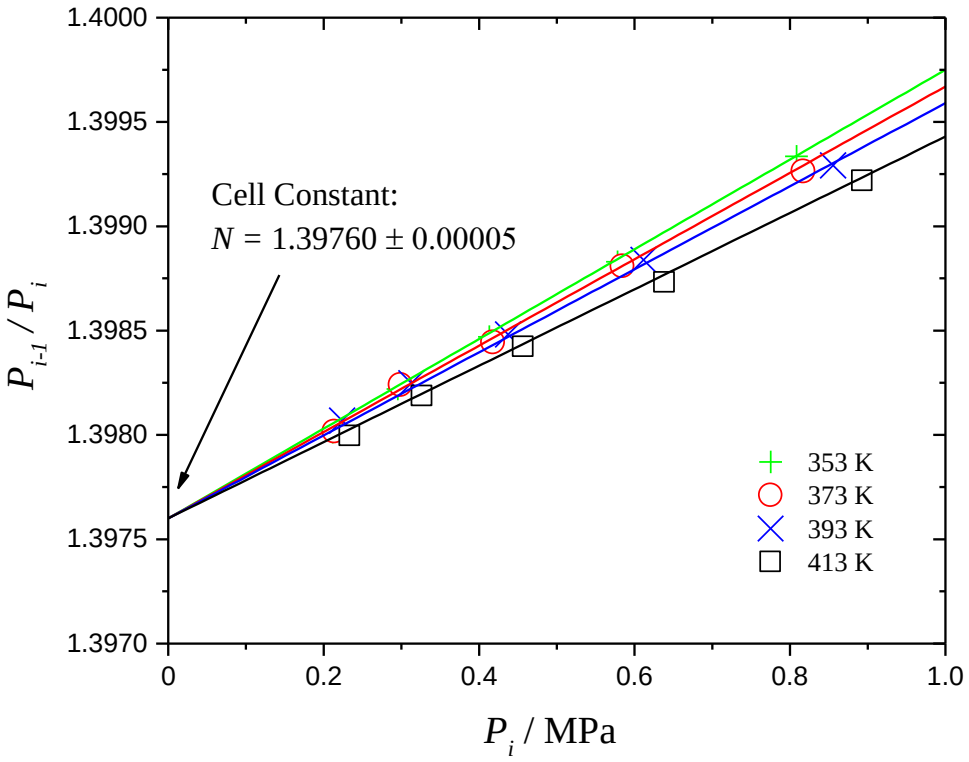

Figure 4.2 Cell constant determined from the PVT measurements of helium

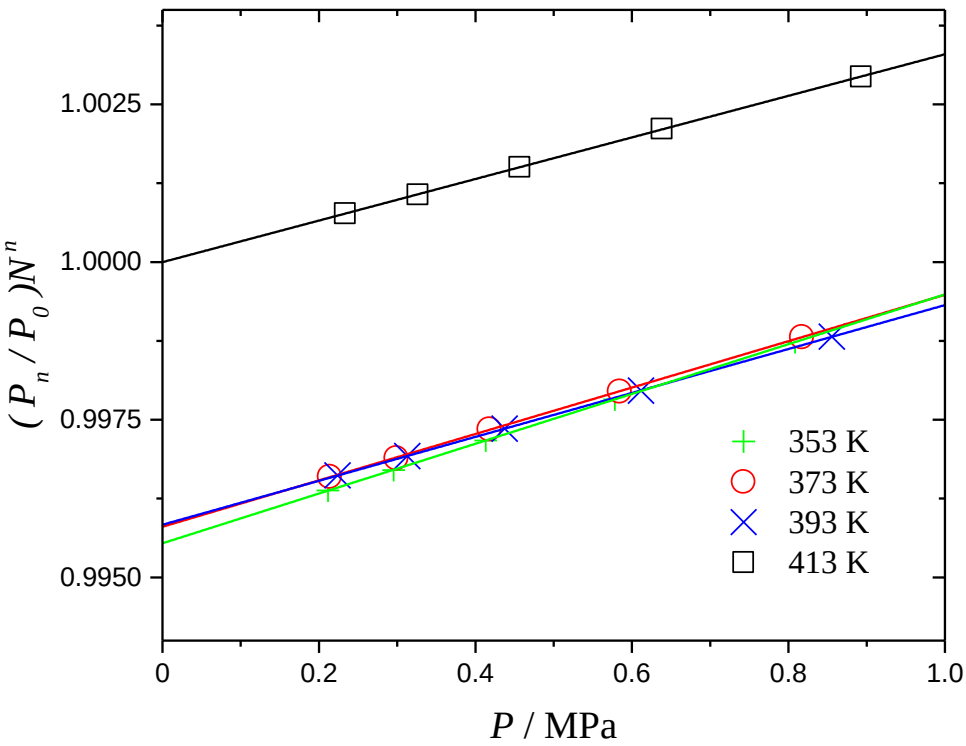

Figure 4.3 Initial compressibility factors of helium from 353 K to 413 K

4.1.2 Comparisons with the EOS by Ortiz-Vega et al.

Ortiz-Vega et al. (2013) [64] gave the newest wide range EOS for helium. This EOS is valid for the temperature range from 2.17 K to 2000 K and pressure up to 2000 MPa which is available for this study. At the temperature over 200 K, the uncertainties in density are 0.02 % up to pressure of 80 MPa which is appropriate to evaluate the present experimental results. The densities of the helium were calculated from REFPROP 9.1 [65] at the same temperatures and pressures and compared with the experimental data. The deviations were within 0.05% which are in good agreement with the EOS as shown in the Fig. 4.4.

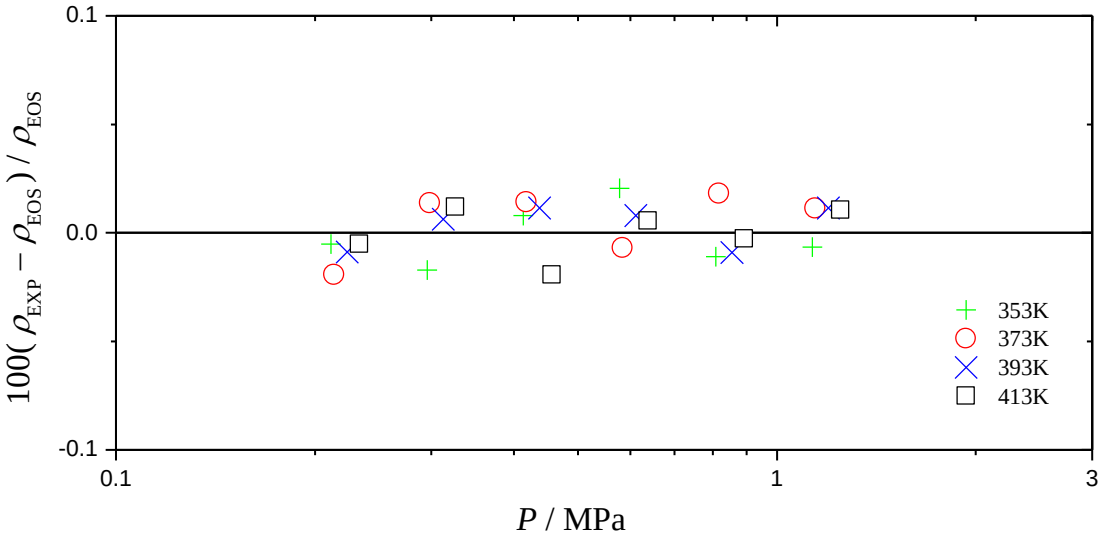

Figure 4.4 Density deviations between the present data and the EOS by Ortiz-Vega et al. [64]

4.2 PVT properties measurements for nitrogen

4.2.1 Experimental results

The PVT properties of nitrogen in the vapor phase were measured at the temperature of 353 K and 413 K in order to verify the reliability of the current apparatus. The initial pressures of nitrogen were 2.42 MPa and 2.55 MPa, respectively. Therefore seven times of expansion were conducted to ensure the final pressure is around 0.2 MPa which is approximately considered as the ideal gas state. The pressures before and after each expansion are shown in the Fig. 4.5. The initial compressibility factors as shown in the Fig. 4.6 of the nitrogen at each temperature were calculated with the cell constant determined from the PVT measurements of helium which have been described above. Densities of nitrogen are evaluated from Eq. 2.11 by utilizing the obtained parameters.

The experimental results are summarized in the Table 4.3.

Table 4.3 Experimental results of PVT properties for nitrogen at 353 K and 413 K

Pressure (MPa)	Density (mol dm^{-3})
T / K=353.172	
2.4252	0.8229
1.7331	0.5888
1.2391	0.4213
0.8861	0.3014
0.6338	0.2157
0.4534	0.1543
0.3244	0.1104
0.2321	0.07900
T / K=413.162	
2.5536	0.7372
1.8226	0.5275
1.3019	0.3774
0.9304	0.2701
0.6651	0.1932
0.4756	0.1383
0.3402	0.09893
0.2433	0.07078

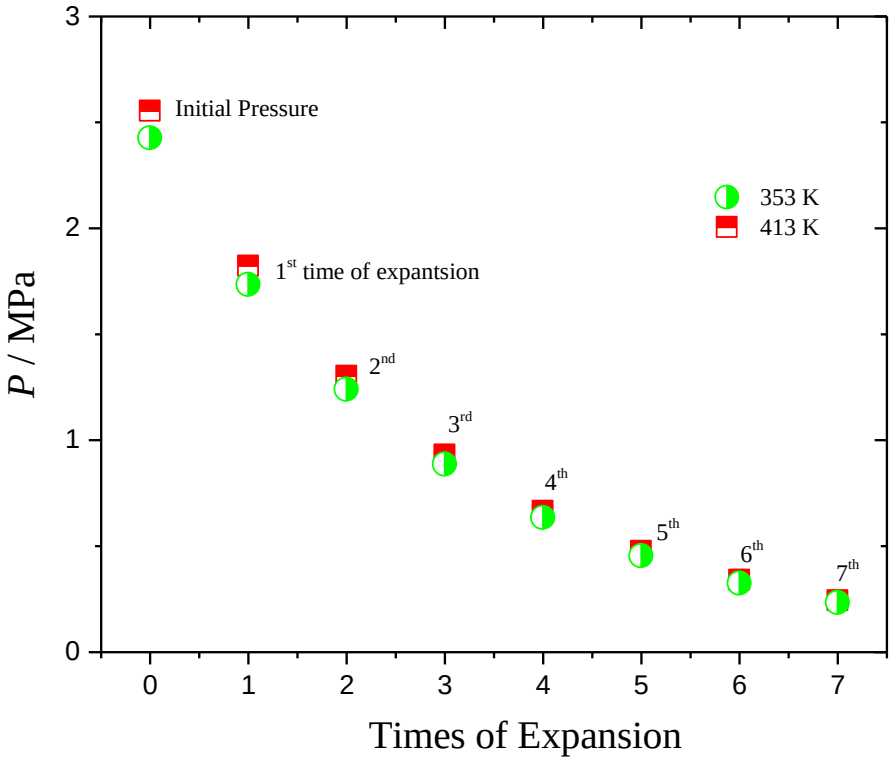

Figure 4.5 Pressures of nitrogen after each expansion

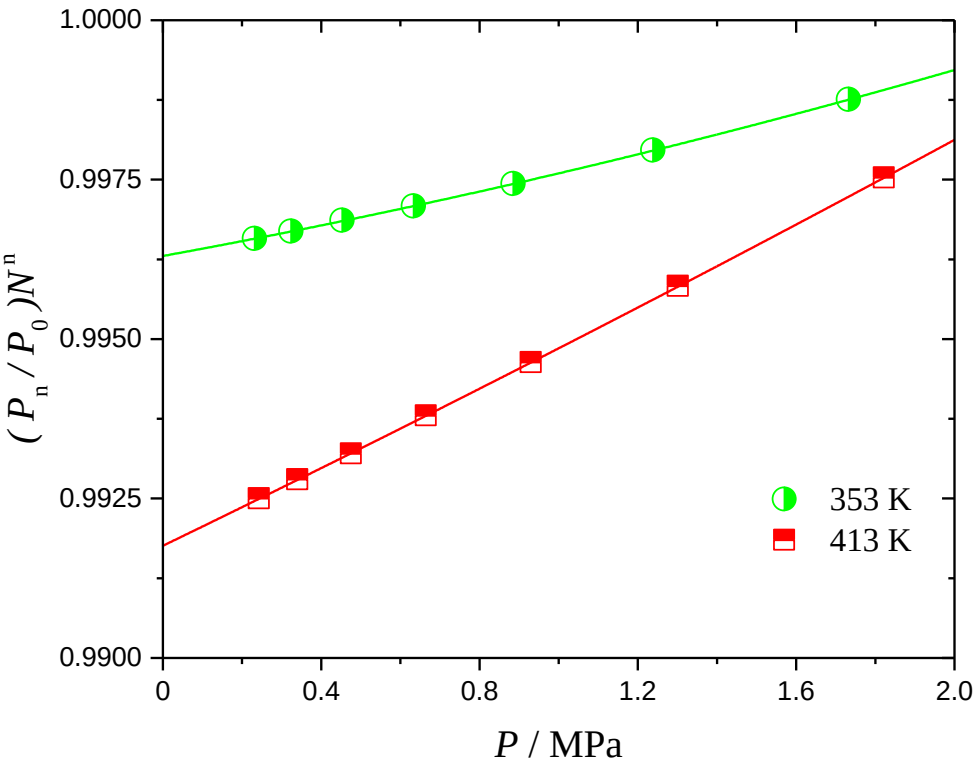

Figure 4.6 Initial compressibility factors of nitrogen at 353 K and 413 K.

4.2.2 Comparisons with the EOS by Span et al.

Span et al. (2000) [66] published a fundamental EOS for the nitrogen. The uncertainty in density at pressures below 30 MPa is 0.02 % which is appropriate to evaluate the present experimental results. For each temperatures, the densities and pressures are calculated from REFPROP 9.1 [65], respectively. The present experimental data are in good agreement with the EOS within 0.1 % as shown in the Fig 4.7 and Fig 4.8.

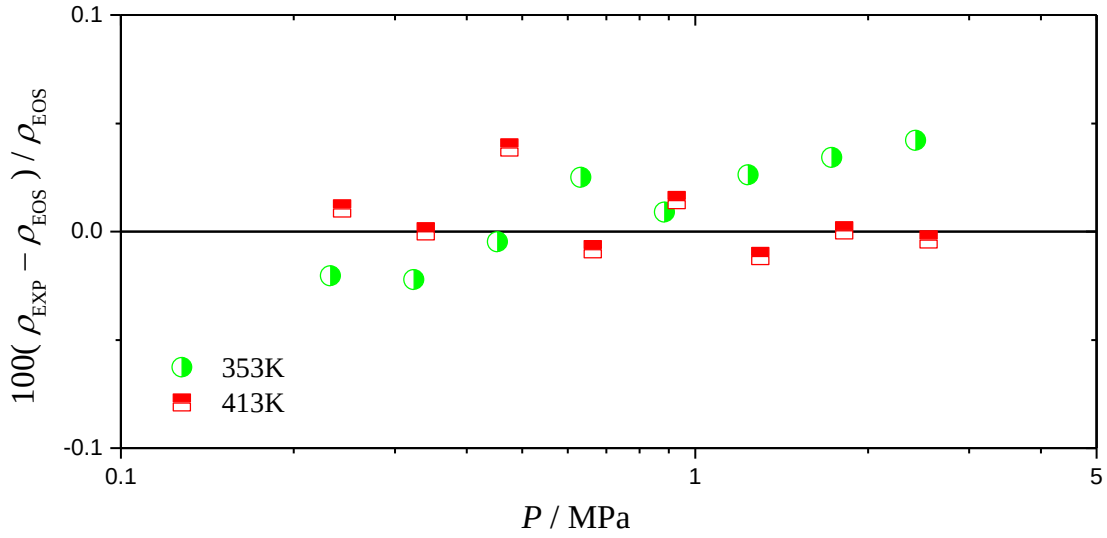

Figure 4.7 The density deviations of nitrogen compared with the EOS by Span et al. [66] at 353 K and 413 K

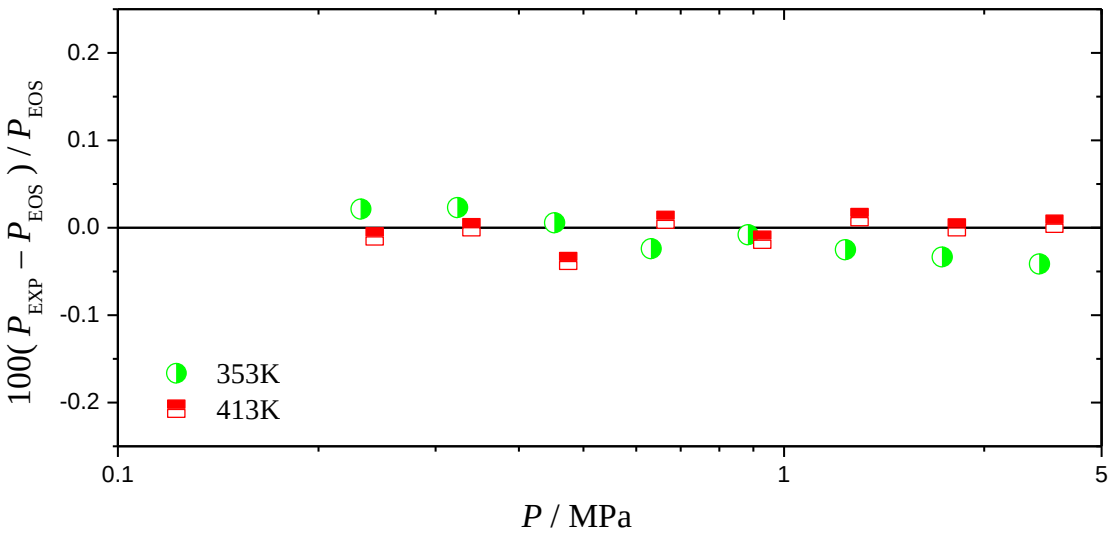

Figure 4.8 The pressure deviations of nitrogen compared with the EOS by Span et al. [66] at 353 K and 413 K

4.3 PVT properties measurements for R134a

4.3.1 Experimental results

Former studies have indicated that the apparatus of Burnett method is appropriate to measure the density of the inorganic substances. However the objective substances of this study are new low GWP refrigerants most of which are organic matters. It is required to verify whether this apparatus is suitable in measuring the refrigerants. Therefore the PVT properties measurements of R134a which is one of the most widely used refrigerant had been carried out at 353 K and 413 K and the initial pressures were 1.76 MPa and 2.61 MPa, respectively. After seven and eight times of expansion, the sample inside the cell were approximate to ideal gas state. Pressures after each time of expansion and the initial compressibility factors are shown in the Fig. 4.9 and Fig. 4.10. Thus, the densities of R134a at each state were calculated based on the Eq. 2.11.

The experimental results are summarized in the Table 4.4.

Table 4.4 Experimental results of PVT properties for R134a at 353 K and 413 K

Pressure (MPa)	Density (mol dm^{-3})
T / K=353.171	
1.7615	0.7767
1.3597	0.5557
1.0260	0.3976
0.7621	0.2845
0.5599	0.2036
0.4082	0.1457
0.2960	0.1042
0.2138	0.07457
T / K=413.165	
2.6068	0.9188
1.9688	0.6574
1.4646	0.4704
1.0776	0.3366
0.7867	0.2408
0.5710	0.1723
0.4128	0.1233
0.2975	0.08822

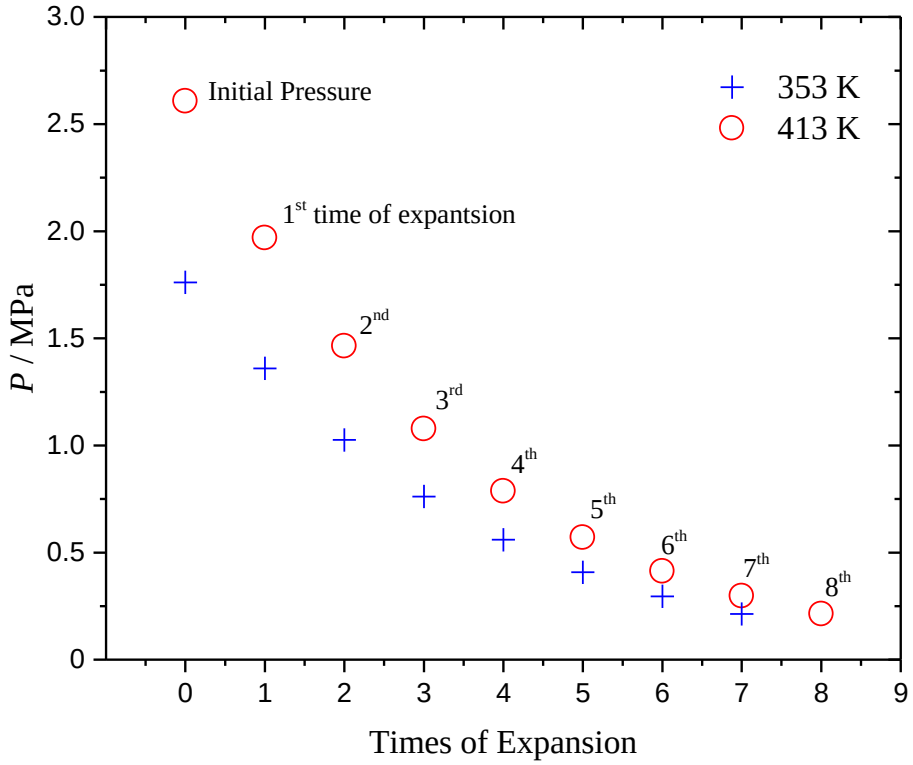

Figure 4.9 Pressures of R134a after each time of expansion.

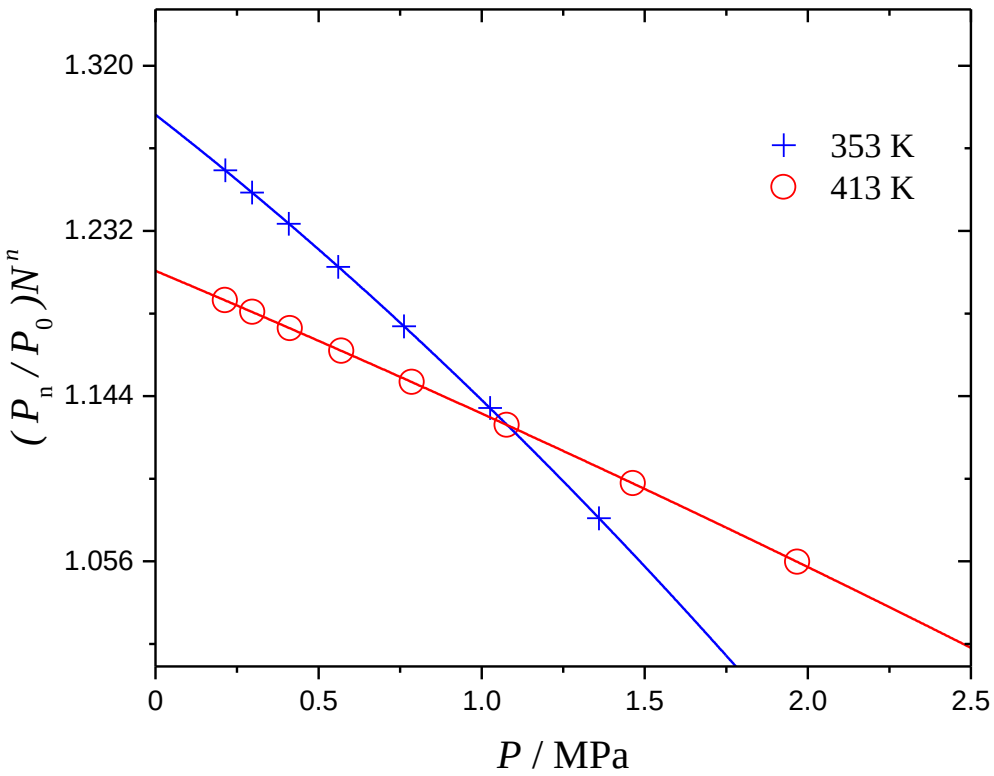

Figure 4.10 Initial compressibility factors of R134a at 353 K and 413 K

4.3.2 Comparisons with Tillner-Roth and Baehr's EOS

Tillner-Roth and Baehr (1994) [67] published a fundamental EOS for the Helmholtz free energy of R134a which is valid at the temperature range from 170 K to 455 K and pressures up to 70 MPa. The accuracy for density evaluation is 0.05 % and 0.02 % for the vapor pressure. Using REFPROP 9.1 [65], the densities and vapor pressures have been calculated and compared with the present experimental results as shown in the Fig. 4.11 and 4.12. The deviations are within 0.1 % for both densities and vapor pressures.

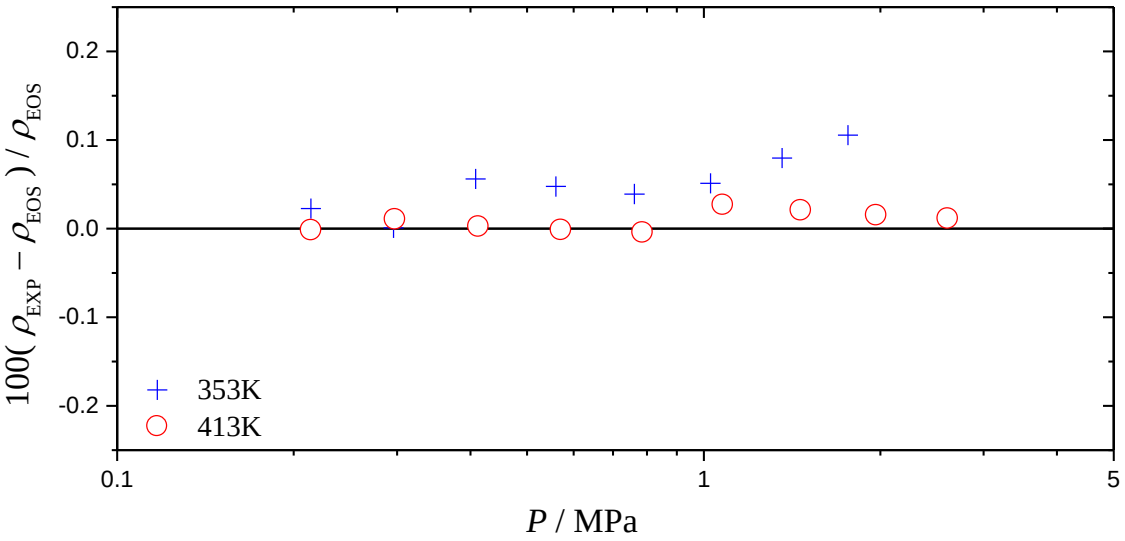

Figure 4.11 The density deviations of R134a compared with the EOS by Tillner-Roth and Baehr [67] at 353 K and 413 K

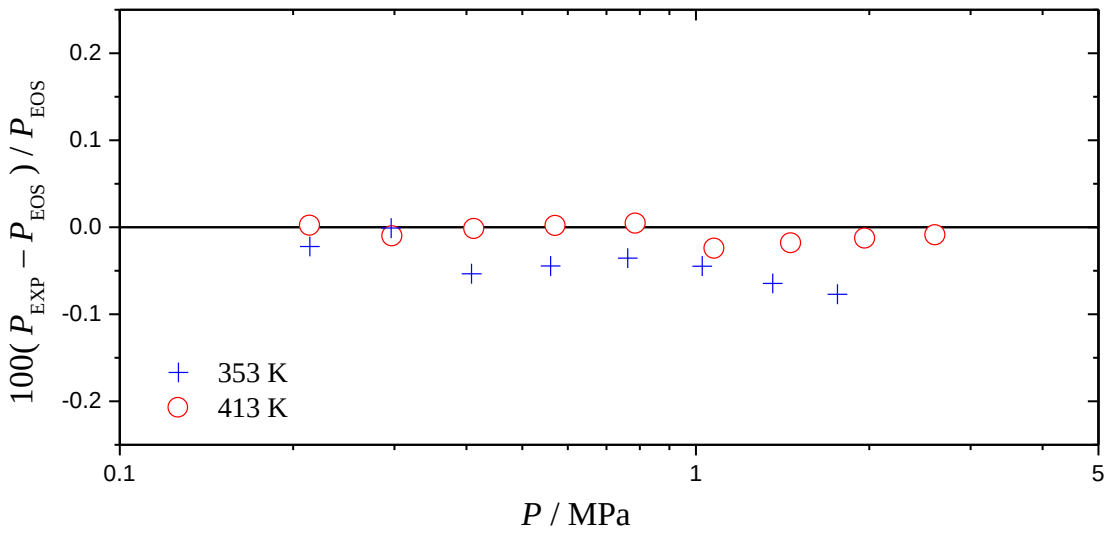

Figure 4.12 The pressure deviations of R134a compared with the EOS by Tillner-Roth and Baehr [67] at 353 K and 413 K

4.4 PVT properties measurement for R1234ze(Z)

4.4.1 Experimental results

The PVT properties measurements for R1234ze(Z) were conducted at the temperature range from 353 K to 413 K at an interval of 20 K and the sample was filled into the sample cell at the vapor-liquid equilibrium state. When the temperature was increased to the target, the saturated condition remained. In this case, the vapor pressures were also obtained. After the measurements of saturate pressure, some amount of the sample was released to transfer the phase to single vapor phase and the PVT measurements were conducted. The initial pressures for each temperatures were 0.74 MPa, 0.96 MPa, 1.84 MPa and 2.73 MPa. Limited by the initial pressures and the features of Burnett method, the expanded times were four, five, seven and nine, respectively. The pressures before and after each expansion are given in the Fig. 4.13. After the initial factors were determined as shown in the Fig. 4.14, the densities of at each condition are summarized in the Table 4.5.

Table 4.5 Experimental results of PVT properties for R1234ze(Z) from 353 K to 413 K

Pressure (MPa)	Density (mol dm^{-3})
T / K=353.165	
0.7391	0.3052
0.5589	0.2184
0.4162	0.1563
0.3063	0.1118
0.2236	0.07999
T / K=373.145	
0.9663	0.3833
0.7346	0.2742
0.5485	0.1962
0.4044	0.1404
0.2956	0.1005
0.2148	0.07188
T / K=393.125	
1.8419	0.8383
1.4810	0.5998
1.1490	0.4292
0.8711	0.3071
0.6492	0.2197
0.4782	0.1572
0.3493	0.1125
0.2536	0.08048
T / K=413.144	
2.7340	1.4320
2.3183	1.0240
1.8703	0.7330
1.4581	0.5244
1.1087	0.3752
0.8283	0.2685
0.6112	0.1921
0.4470	0.1375
0.3249	0.09835
0.2351	0.07037
0.2336	0.06795

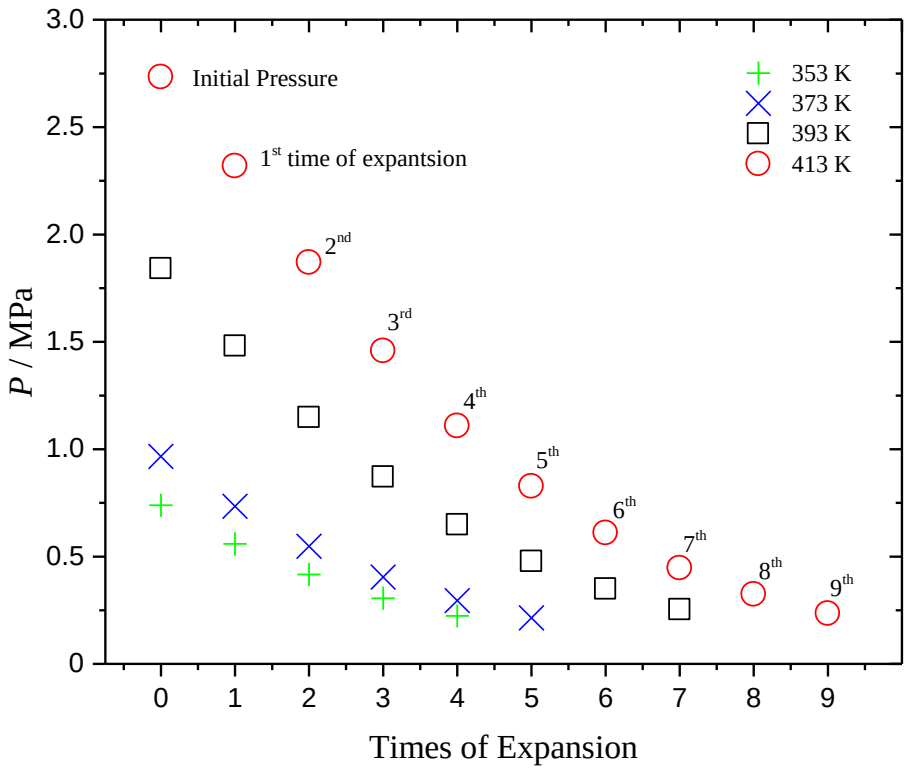

Figure 4.13 Pressures of R1234ze(Z) after each time of expansion.

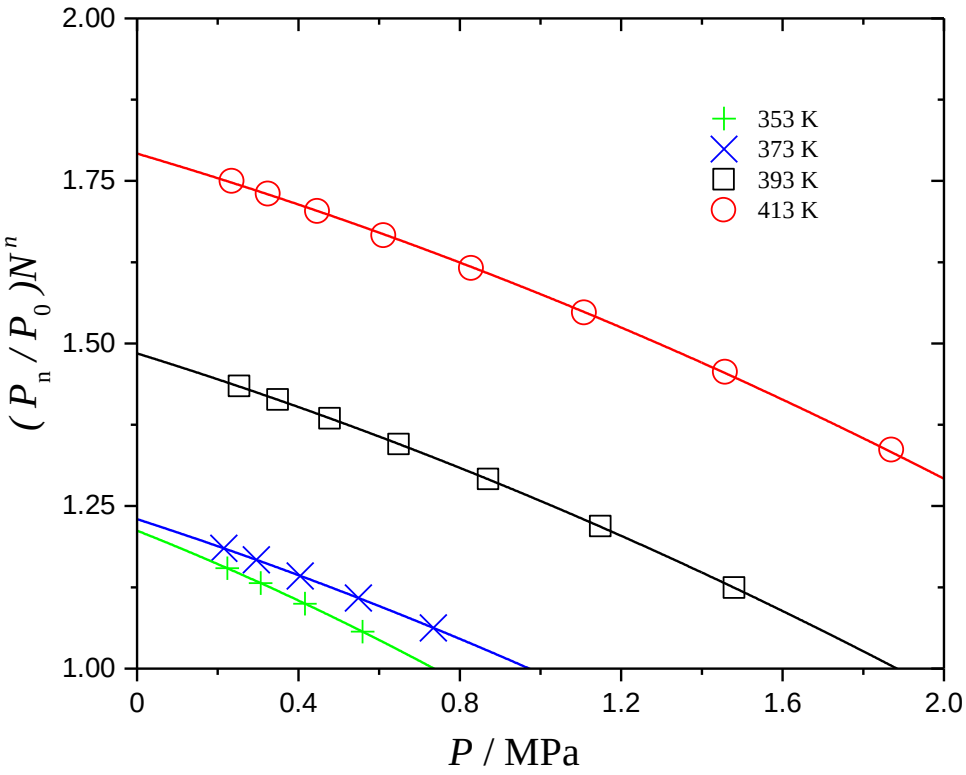

Figure 4.14 Initial compressibility factors of R1234ze(Z) from 353 K to 413 K

4.4.2 Comparisons with other published data and the EOS by Akasaka et al.

The vapor pressures are compared with the EOS by Akasaka et al. (2014) [68] and other published data as shown in the Fig. 4.15 and Fig. 4.16. The percentage deviations of the present data are within 0.1 % and the absolute deviations are within 3 kPa. The EOS represents other published vapor pressures data from Higashi et al. (2013) [22] and Tanaka et al. (2013) [25] within 0.2 % and 5 kPa. The present data are consistent with Tanaka et al.'s experimental data. In the low temperature range from 280 K to 330 K, Fedele et al.'s (2014) [21] data show larger percentage deviations compared with the EOS within 0.5 % due to the low pressures and the absolute deviations are in good agreement with the EOS within 2 kPa.

For the measurements of PVT properties, the densities and pressures deviations are given in the Fig. 4.17 and Fig. 4.18 compared with the EOS by Akasaka et al. [68]. The other published data by Fedele et al. [21] and Higashi et al. [22] are also plotted in the figures in the temperature range from 360 K to 415 K and pressures up to 6 MPa. As shown in the figures, the available PVT properties data are insufficient and the present data are in the region between Fedele et al.'s and Higashi et al.'s data. The density deviations of the present data are within 0.3 % except for the points close to the vapor pressures at 413 K in Fig. 3.17. The pressure deviations are within 0.2 % and smaller at pressures close to the vapor pressures at 413 K in Fig. 4.18. The difference between the present data and the calculation results are slightly larger than the uncertainty of the measurement at some data points, therefore the EOS could be improved by fitting the present data.

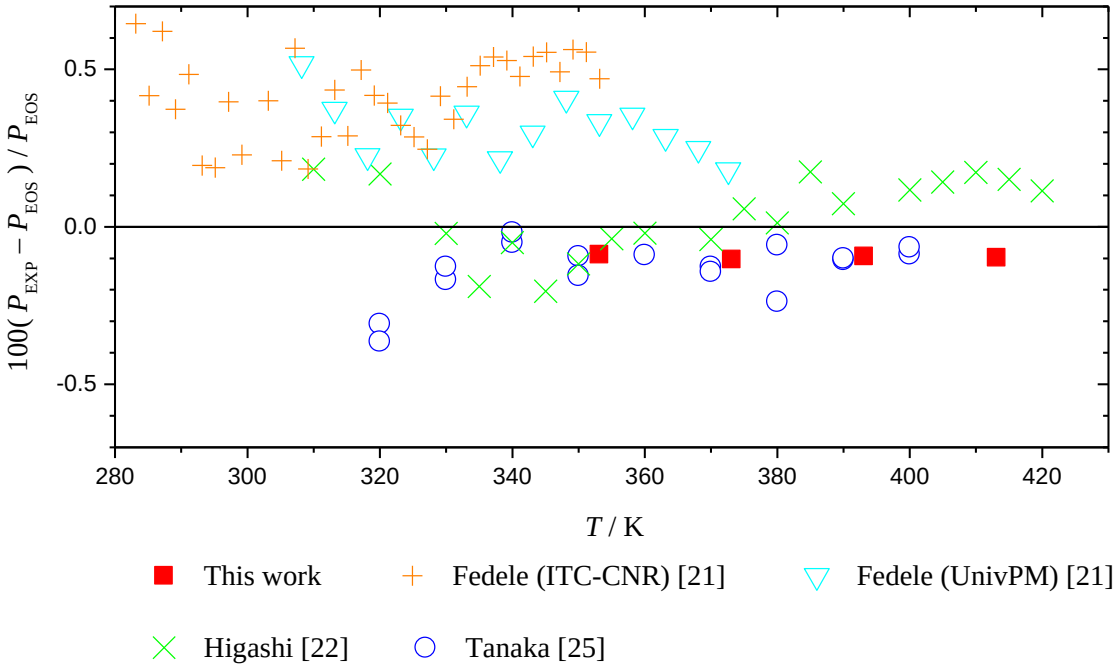

Figure 4.15 Percentage deviations of vapor pressure for R1234ze(Z) between experimental data and EOS by Akasaka et al. [68]

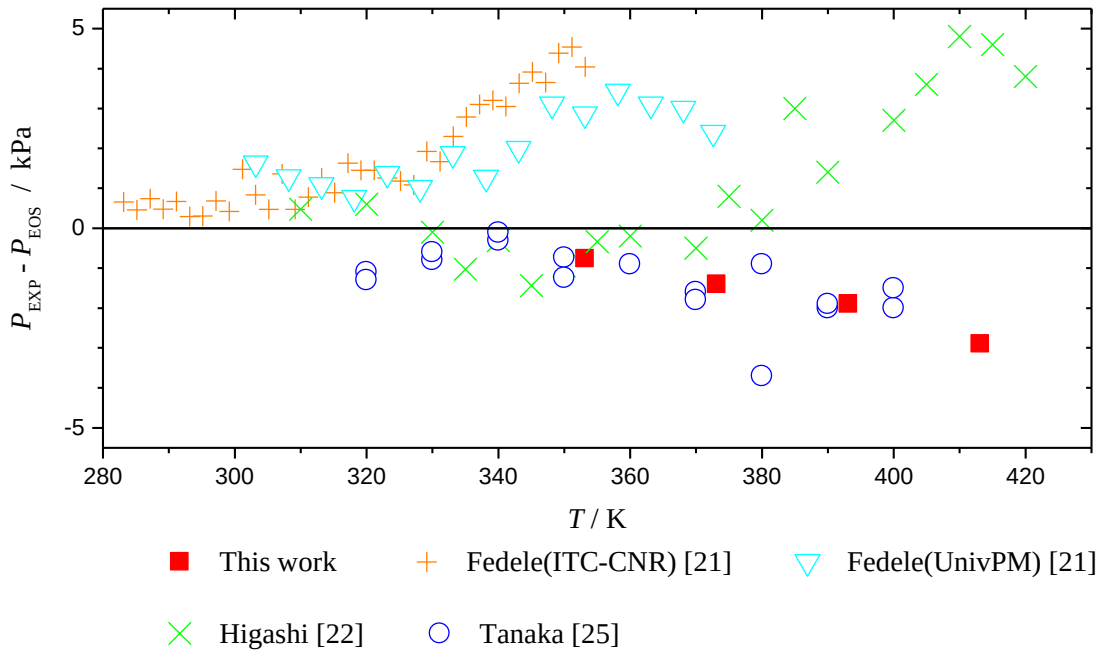

Figure 4.16 Absolute deviations of vapor pressure for R1234ze(Z) between experimental data and the EOS by Akasaka et al. [68]

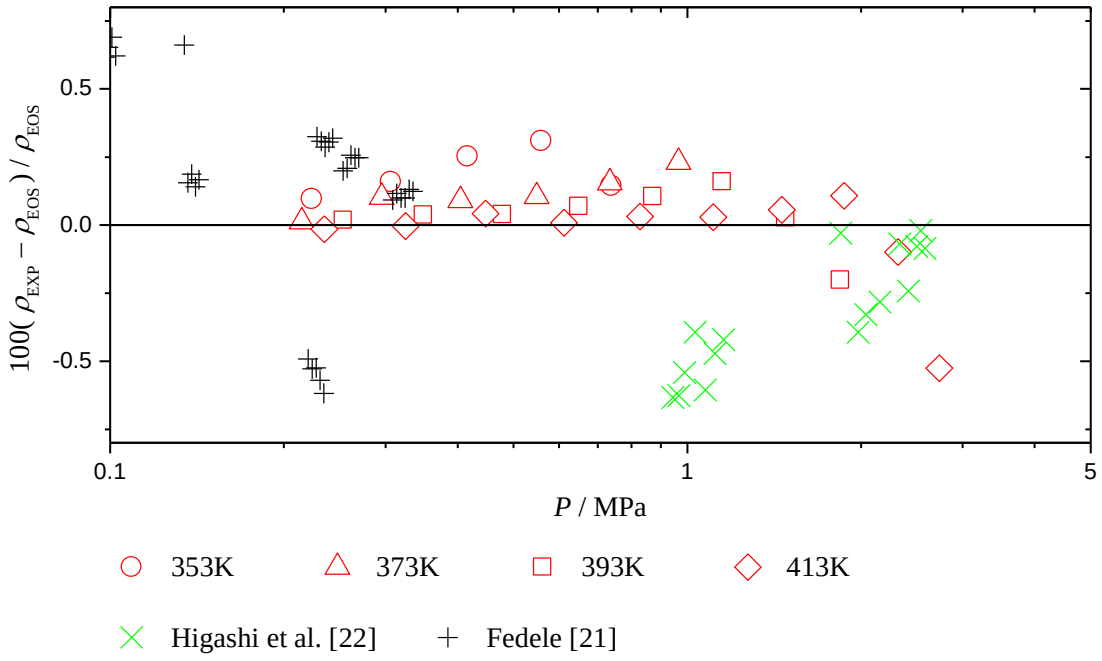

Figure 4.17 Density deviations of PVT properties for R1234ze(Z) between experimental data and the EOS by Akasaka et al. [68]

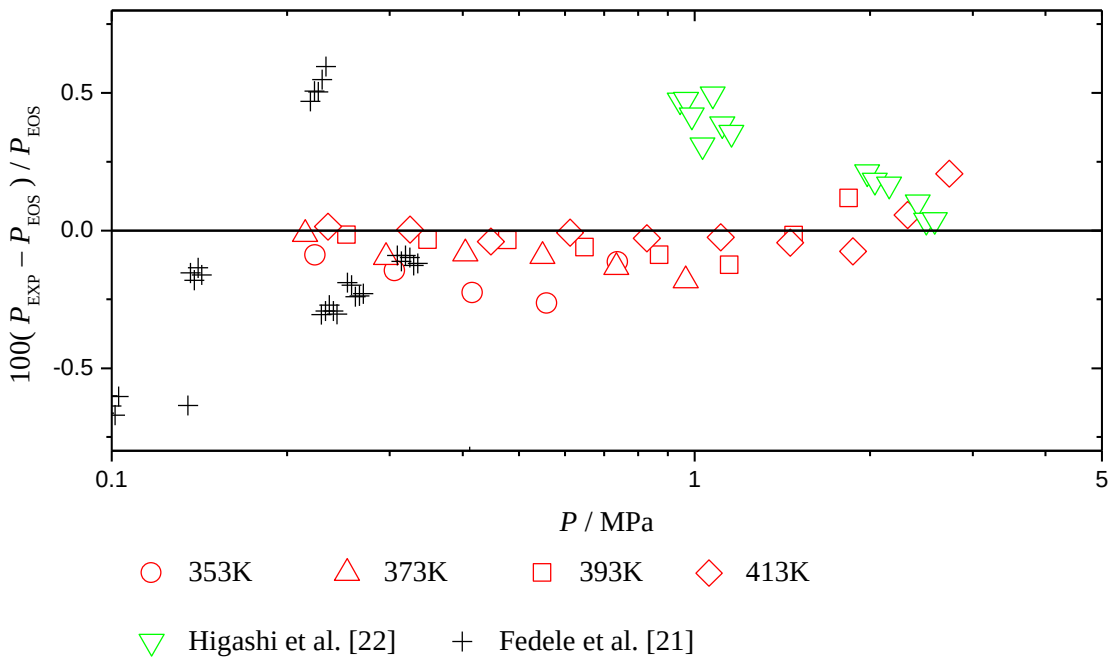

Figure 4.18 Pressure deviations of PVT properties for R1234ze(Z) between experimental data and the EOS by Akasaka et al. [68]

Chapter 5 Experimental Results on VLE Properties

In this chapter, the experimental VLE data of the binary mixture of R32 + R1234yf are described and compared with the existing mixing models to verify the reliability of the new assembled apparatus. And the binary mixtures of R32 + R1123 and R1123 + R1234yf have been measured at different concentrations and compared with mixing models with default parameters. The samples used in this experiment are produced by Asahi Glass Co., Ltd. Japan and the information is given in the Table 5.1.

Table 5.1 Information of the samples

Sample	Purity	Manufacturer
R32	99.96 %	
R1234yf	99.91 %	Asahi Glass Co., Ltd.
R1123	99.93 %	

5.1 VLE properties for binary mixture of R32 + R1234yf

5.1.1 Experimental results

The binary mixture of R32 + R1234yf was filled into the equilibrium cell at vapor liquid equilibria condition. The experimental temperatures are from 283 K to 313 K at an interval of 10 K and the pressures have been measured at each temperature. The results of compositions from gas chromatograph were converted to mass fraction by Eq. 3.3 and the concentration of the R32 was 60 % in mass fraction. Total eight PTxy experimental data points were obtained and summarized in the Table 5.2.

Table 5.2 VLE Data of the R32 + R1234yf Mixtures

T / K	*P* / MPa	Mass Fraction of R32	
		Liquid	Vapor
283.15	1.0067	0.5930	0.6558
293.09	1.3382	0.5867	0.6964
303.19	1.7398	0.5742	0.6945
313.27	2.2204	0.5644	0.6864

5.1.2 Comparisons with the EOS and other published data.

The EOS of pure R32 was reported by Tillner-Roth et al. (1997) [69] available at temperature from 136.34 K to 435 K and pressures up to 70 MPa. For the pure R1234yf, Richter et al. (2011) [70] presented the EOS at temperature region between 240 K to 320 K and pressures up to 10 MPa. Kunz et al. (2012) [71] has developed a widely-range mixing model to calculate the VLE properties. For the mixture of R32 + R1234yf, Akasaka (2013) [72] determined the mixing parameters based on the experimental data from Kamiaka et al. [38]. The *P*-*x* and *x*-*y* diagrams are shown in the Fig. 5.1 and Fig. 5.2 with the published data from Kamiaka et al [38]. The present data are in agreement with the mixture model within 1.1 % except for the dew pressure point at 273 K and Kamiaka et al.'s data show the same magnitude of deviations at the concentrations of 50 and 70 % as shown in the Fig. 5.3. Considering the accuracy of the EOS, the deviations of the experimental results are acceptable.

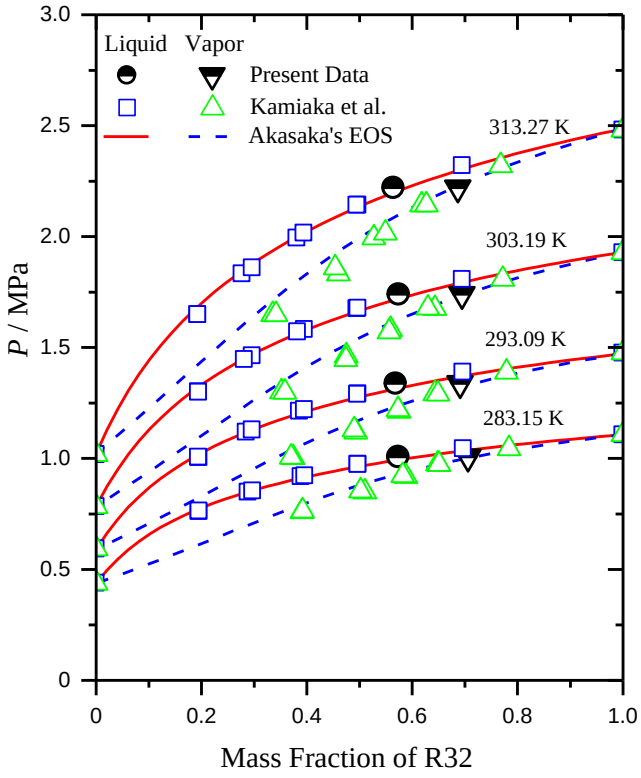

Figure 5.1 Distribution of VLE experimental results of R32+R1234yf

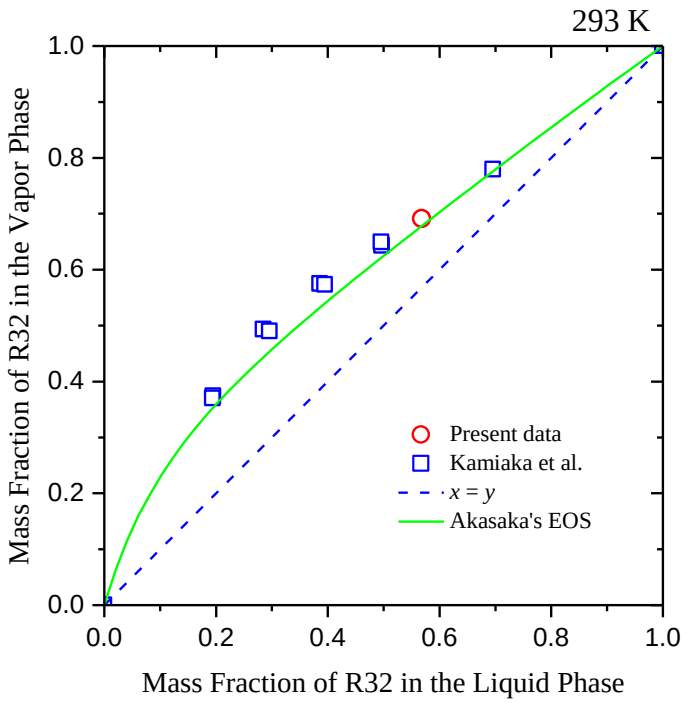

Figure 5.2 Mass fraction of R32 in the liquid and vapor phase

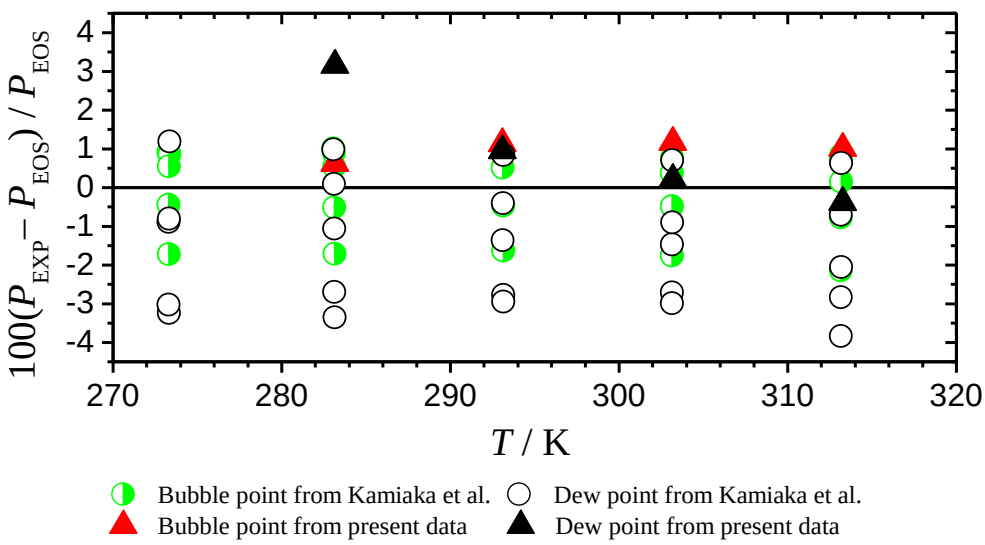

Figure 5.3. Deviations for bubble point pressures between experimental data and mixing model with the parameters from Akasaka [72].

5.2 VLE properties for the binary mixture of R32 + R1123

5.2.1 Experimental results

The VLE properties of R32 + R1123 mixture were measured at the temperature range from 273 to 313 K at a step of 10 K. The composition of this mixture was measured from the results of gas chromatograph by Eq. 3.1. The concentrations of R32 were 45 % and 60 % and twenty experimental data points are summarized in the Table 5.3.

Table 5.3 VLE Data of the R32 + 1123 Mixtures

T / K	*P* / MPa	Mass Fraction of R32	
		Liquid	Vapor
(45/55)			
273.22	1.0319	0.4572	0.4001
283.43	1.3865	0.4534	0.4039
293.35	1.8080	0.4565	0.4161
303.53	2.3468	0.4659	0.4319
313.24	2.9485	0.4667	0.4318
(60/40)			
273.22	0.9759	0.6210	0.5666
283.43	1.3222	0.6166	0.5467
293.30	1.7320	0.6209	0.5575
303.54	2.2578	0.6118	0.5563
313.24	2.8401	0.6162	0.5681

5.2.2 Comparisons with the EOS by Akasaka

Since there is no valid data utilized to determine the mixing parameters, an EOS based on the simulated data was reported by Akasaka (2016) [73]. The EOS of pure R1123 was reported by Akasaka et al. [74]. By applying the mixing model, the VLE properties can be calculated and presented in the $P - x$ and x-y diagram as shown in the Fig. 5.4 and Fig 5.5. The dew point and bubble point pressures were evaluated and compared to the present data. The deviations are shown in the Fig. 5.6. The present data are in agreement with the EOS within 2.5 % at bubble and dew point pressures,

respectively. The deviations reduce as the temperature rises. At 313 K the deviations are within 0.5 % while at 273 K the deviations are larger than 2.5 %. One of the reasonable explanation is that the accuracy of the EOS for the pure R1123 developed by Akasaka et al. [74] reduced at low temperature range due to the lack of valid experimental data.

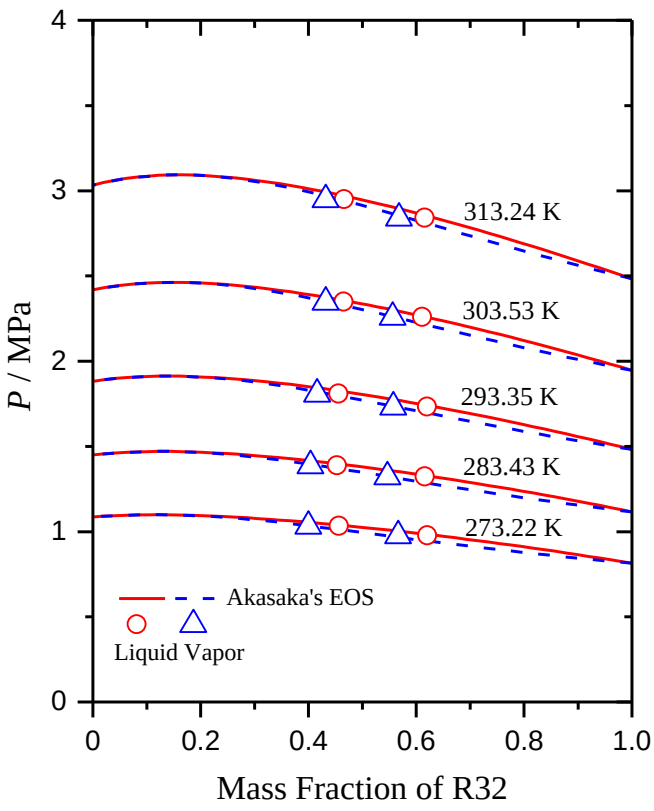

Figure 5.4 *P-x* diagram for the binary mixture of R32 + R1123

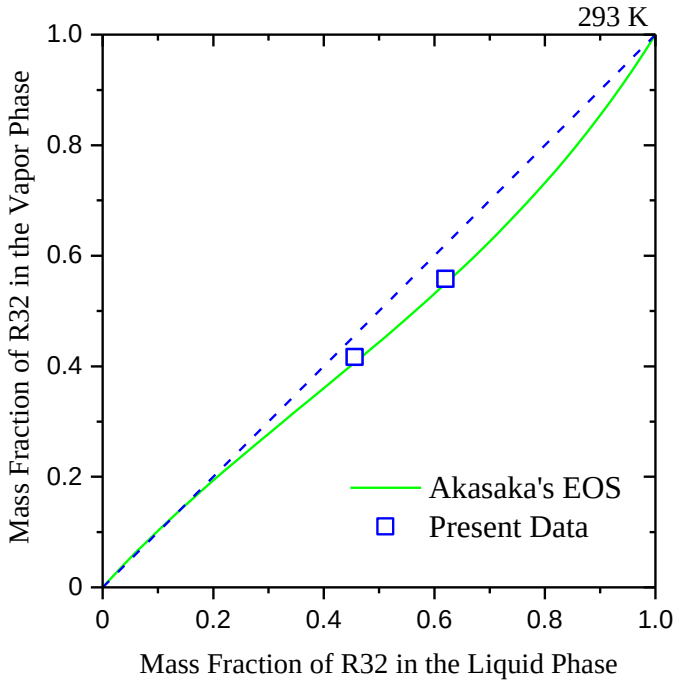

Figure 5.5 Mass fraction of R32 in the liquid and vapor phases

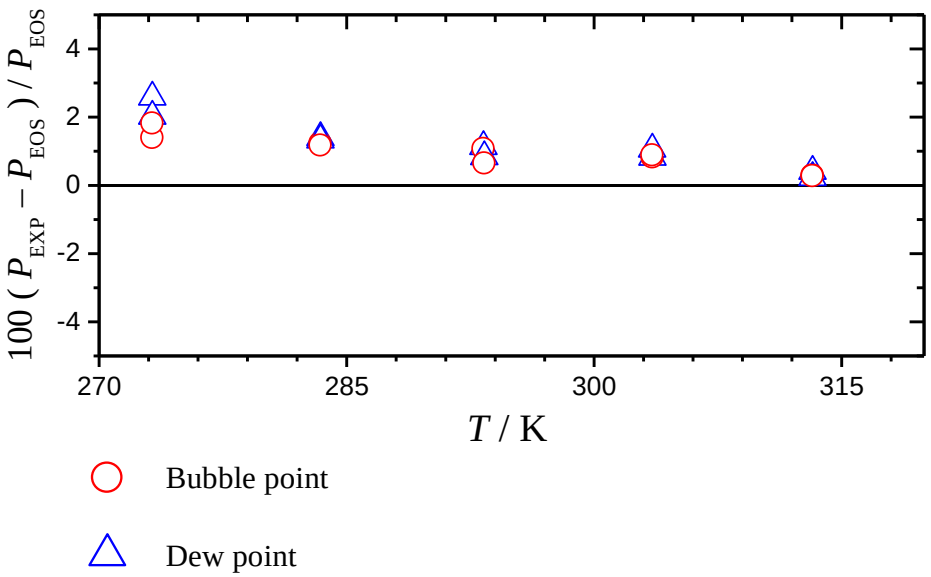

Figure 5.6 Pressure deviations between the present data and the EOS by Akasaka [73]

5.3 VLE properties for the binary mixture of R1123 + R1234yf

5.3.1 Experimental results

The binary mixtures of R1123 + R1234yf with three different compositions were measured at the temperature ranging from 273 K to 313 K at an interval of 10 K. The mass fractions were calculated from the results of gas chromatograph based on Eq. 3.5 and the concentrations of R1234yf were 50 %, 75 % and 80 %. Total thirty experimental data points were obtained and summarized in the Table 5.4.

5.3.2 Comparison with the EOS with default mixing parameters

There is no valid experimental data of the binary mixture of R1123 + R1234yf to determine the mixing parameters for the mixing model. Therefore in this study, the KW0 mixing model with default mixing parameters was used to calculate the VLE properties by REFPROP 9.1 [65]. The *P*-*x* and *x*-*y* diagrams are shown in the Fig 5.7 and Fig 5.8 and the deviations of the bubble and dew point pressures are shown in the Fig 5.9.

Table 5.4 VLE Data of the R1234yf+R1123 Mixtures

T / K	*P* / MPa	Mass Fraction of R1234yf	
		Liquid	Vapor
(50/50)			
273.21	0.7083	0.5419	0.3405
283.14	0.9349	0.5154	0.3663
293.03	1.1976	0.5591	0.4159
303.13	1.5200	0.5725	0.4202
313.21	1.8726	0.5965	0.4444
(80/20)			
273.24	0.5266	0.7309	0.5818
283.13	0.6529	0.8019	0.6576
293.02	0.8806	0.7870	0.6597
303.13	1.0997	0.8196	0.6700
313.81	1.4042	0.8228	0.6695
(75/25)			
273.26	0.5202	0.7676	0.5927
283.25	0.6834	0.7836	0.6203
293.05	0.9106	0.7815	0.6420
303.25	1.1466	0.7958	0.6624
313.24	1.4427	0.8039	0.6906

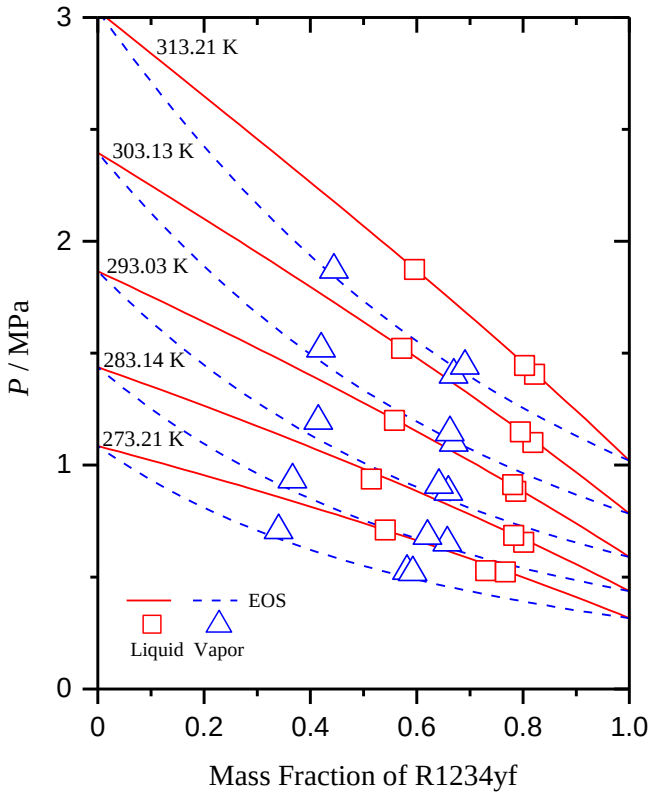

Figure 5.7 *P-x* diagram for the binary mixture of R1234yf + R1123

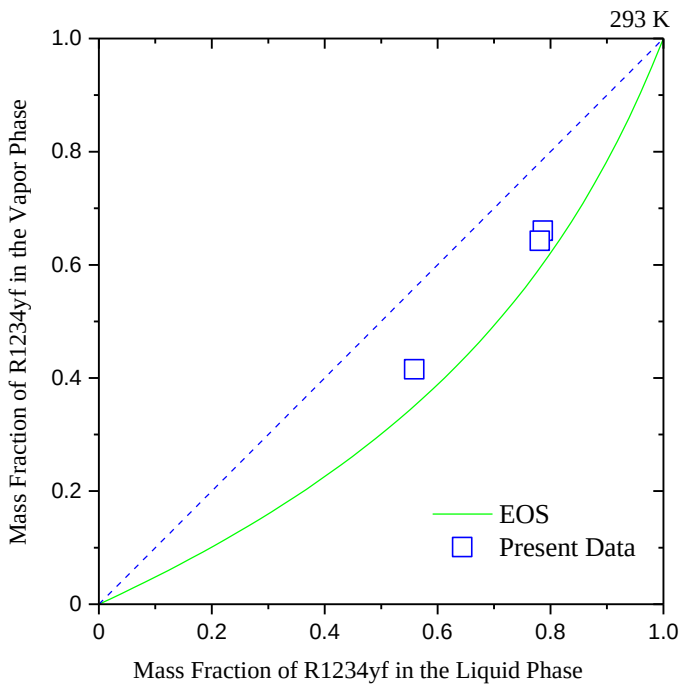

Figure 5.8 Mass fraction of R1234yf in the liquid and vapor phases

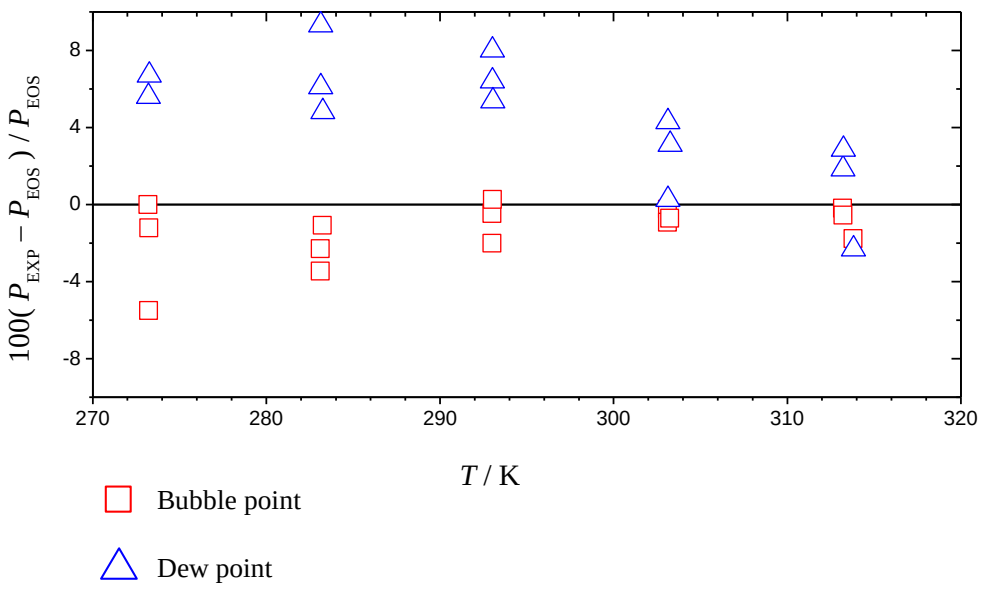

Figure 5.9 Pressure deviations between the present data and the EOS with default mixing parameters.

The deviations of the bubble point pressures are smaller than dew point at each temperature. For the bubble point pressure, the deviations are within 3.5 % except for the point at 273 K with 80 % of R1234yf. For the dew point pressures, the deviations vary from 0.2 % to 11 %. The deviations are much larger than the uncertainties of this experiment.

5.4 Discussion

Measured data of R32 + R1123 and R1123 + R1234yf were correlated with the Peng-Robinson (PR) type of equation of state.

The PR equation [75] is expressed as follows:

$$P = \frac{RT}{v-b} - \frac{a(T)}{v(v+b)+b(v-b)} \tag{5.1}$$

With

$$a(T) = 0.45724\frac{R^2T_c^2}{P_C}\left\{1+\kappa\left(1+\sqrt{\frac{T}{T_C}}\right)\right\}^2 \tag{5.2}$$

$$\kappa = 0.37464 + 1.54226\omega - 0.26992\omega^2 \tag{5.3}$$

$$b = 0.07780\frac{RT_C}{P_C} \tag{5.4}$$

Where a and b are energy and size parameters, respectively. R is the universal gas constant. T, P, and v are temperature, pressure, and molar volume, respectively. ω is the acentric factor. T_c and P_c are the critical temperature and pressure.

For multi-component mixtures, the following mixing rule is used

$$a_m = \sum_i\sum_j x_i x_j a_{ij}, \quad b_m = \sum_i x_i b_i \tag{5.5}$$

$$a_{ij} = (1-k_{ij})\sqrt{a_i a_j}, \quad (k_{ij} = k_{ji}) \tag{5.6}$$

Where x_i is the concentration of ith component. Subscripts m, i, and j indicate the value of the mixture, component i, and component j, respectively. k_{ij} is the binary interaction parameter and is generally determined by fitting the measured VLE data. The substance constants used in the calculation is shown in the table 5.5.

For a binary mixture, Eqs. 5.5 and 5.6 can be expressed as follows:

$$a_m = x_1^2 a_1 + x_2^2 a_2 + 2(1-k_{12})\sqrt{a_1 a_2} \tag{5.7}$$

$$b_m = x_1 b_1 + x_2 b_2 \tag{5.8}$$

In this thesis, binary interaction parameters k_{ij} was optimized by fitting to measured VLE data. The objective function in optimization is as follows:

$$E = \sum \left(\frac{P_{\text{exp}}}{P_{\text{cal}}} - 1\right)^2_{\text{bubble}} + \sum \left(\frac{P_{\text{exp}}}{P_{\text{cal}}} - 1\right)^2_{\text{dew}} \tag{5.9}$$

Table 5.5 Substance constants of R32, R1123 and R1234yf

Property	R32 [76]	R1123 [56]	R1234yf [29]
Molar mass (g mol^{-1})	52.023	82.025	114.04
Critical temperature (K)	351.26	331.73	367.85
Critical pressure (MPa)	5.782	4.543	3.382
Acentric factors	0.278	0.261	0.276

k_{ij} for the binary mixtures of R32 + R1132 and R1123 + R1234yf were determined to be 0.0307 and 0.0102, respectively.

Using optimized parameters in the EOS, saturated pressures were calculated and compared with measured values. Results are shown in the Fig 5.10 and 5.11. The PR EOS can successfully represent saturated pressure and reduce the deviation compared with existing EOS. For the mixture of R32 + R1123, the present data agree with the optimized PR EOS within 1.5 %. For the mixture of R1123 + R1234yf, the deviations of the saturation pressures are within 6 % compared with the optimized PR EOS.

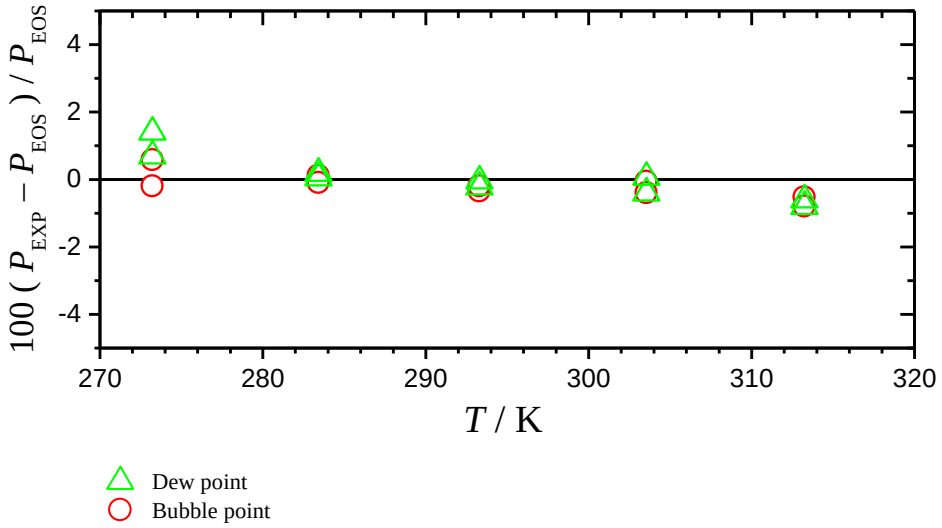

Figure 5.10 Deviations of the present data of R32 + R1123 from optimized PR EOS

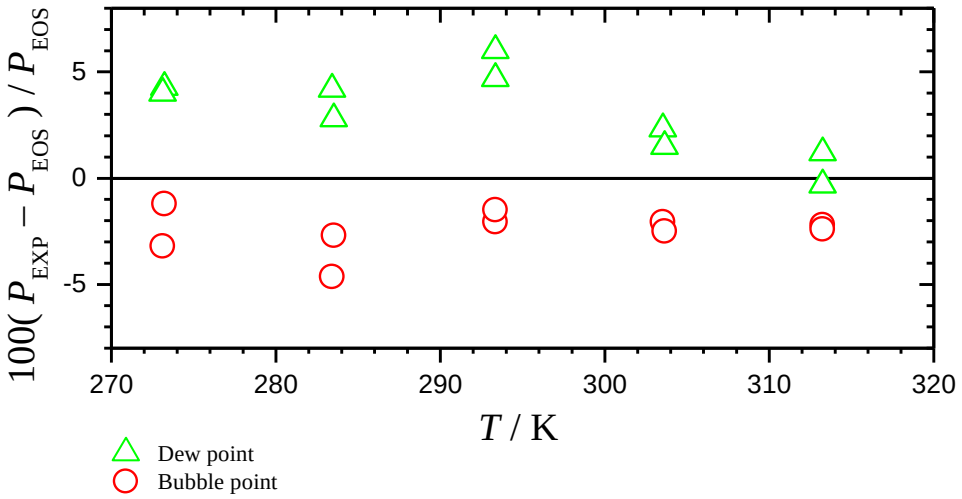

Figure 5.11 Deviations of the present data of R1123 + R1234yf from optimized PR EOS

Chapter 6 Conclusions

The primary objective of the thesis is to investigate the PVT and VLE properties of new low GWP HFOs and their blends. The PVT properties measurement is for those HFOs which will be used in the high temperature heat pump systems and the VLE properties measurement is for the ones which will be utilized in the low temperature heat pump system.

In Chapter 1, the background of the study is introduced, the global warming problem is the main motive force to investigate new refrigerants. Among all of this candidates the HFOs are expected to be the promising alternatives. The thermodynamic properties of three kinds of HFO refrigerants which are studied in this thesis and the blends with some other substances are introduced and presented based on the literature review. Through the review, we realized that one of the limitations for developing the applications is the lack of accurate experimental data. The historical development is discussed and some of the representative refrigerants are shown. The numbering scheme of the refrigerants is presented.

In Chapter 2, the background of the Burnett method for PVT properties measurements is introduced. The basic principle and mathematical analysis are presented. The detailed description of the apparatus is presented. The calibration of temperature is also given based on the ITS90. The procedures of the operations and the supplying method for some refrigerant with high boiling temperature and low pressure are described. The uncertainty of this measurements is estimated.

In Chapter 3, the details of the apparatus used in the VLE properties measurement are presented. The results of the gas chromatograph are shown in a schematic diagram.

For the composition measurement, the conversion factors are determined by measuring the standard binary mixtures of R32, R1123 and R1234yf. Uncertainties of the experiments are evaluated. The procedures of the experiment are discussed.

In Chapter 4, the information on the sample utilized in the PVT properties measurement are shown. Extensive experimental results are presented to confirm the reliability of the experimental apparatus. The data of helium, nitrogen, R134a and R1234ze(Z) are presented and compared with some existing EOS and published data.

(1) Helium was measured at the temperatures of 353 K, 373 K, 393 K and 413 K. Based on the results the cell constants were calculated as 1.39760 ± 0.00005. The experimental data are compared with EOS and the deviations are within 0.05 %.

(2) Nitrogen and R134a were measured at the temperatures of 353 K and 413 K. The density and pressure are compared with the EOSs and show the same magnitude of deviations within 0.1 %. The present experimental results agree well with the EOSs.

(3) R1234ze(Z) was filled into the sample cell at the vapor-liquid equilibrium state. The vapor pressure and single gaseous PVT properties were measured at the temperatures of 353 K, 373 K, 393 K and 413 K. The results were compared with the existing EOS and published data. Our data agree well with the Akasaka EOS within 0.1 % in vapor pressure and show the deviations within 0.3 % in density except for the one close to the vapor density at 413 K. Therefore, in the temperature region of this experiment, our data could be used as the database to increase the accuracy of the Akasaka EOS.

In Chapter 5, the information on the samples used in the measurement of VLE properties is presented. Based on the conversion functions determined in chapter 3, the

compositions of the binary mixtures were calculated from results of gas chromatograph. The binary mixture of R32 + R1234yf, R32 + R1123 and R1123 + R1234yf were measured and compared with existing data and existing EOS.

(1) R32 + R1234yf was measured at the temperature between 283 K and 313 K at an interval of 10 K. The experimental results were compared with the Kamiaka et al.'s [25] data and the EOS by Akasaka et al. for the bubble point pressure and dew point pressure. The present data agree with the EOS within 4 % and Kamiaka et al's data show the same magnitude at similar mass fraction.

(2) R32 + R1123 were measured at the temperature between 273 K and 313 K at a step of 10 K. The experimental results were compared with Akasaka EOS for bubble and dew point pressures with mixing parameters determined by fitting simulated data. The Akasaka EOS represents the saturation pressure of the experimental data within 3 %. The experimental data were correlated with PR equation and the interaction factor was determined to be 0.0307. The optimized PR EOS shows the deviation for saturation pressure from present data within 1.5 %.

(3) R1123 + R1234yf were measured at the temperature between 273 K and 313 K at a space of 10 K. The VLE properties of three different compositions were obtained and compared with the KW0 mixing model with default mixing parameters for bubble and dew point pressures. The deviations for the bubble point pressure are within 3.5 % except for the point at 273 K with 80 % of R1234yf, and for the dew point pressures the deviations are within 11 %. The data were also correlated with PR equation and the interaction factor was determined as 0.0102. Our experimental data agree with the optimized PR EOS within 6 % for both bubble and dew point pressures.

As an overall conclusion, this study presents an experimental investigation of VLE

and PVT properties measurements for low GWP refrigerants and their mixtures. The results in this study would be an evidence to evaluate the reliability of existing EOS and be a supplement of the database to develop it. The work we did contributes to finding better low refrigerants and the coming low-carbon society.

Reference

[1] Hansen, J.; Ruedy, R.; Sato, M.; Lo, K. Global surface temperature change. *Rev. Geophys*, 2010, 48, RG4004.

[2] Perkins, J. Apparatus for producing ice and cooling fluids. Patent 6662, 1834, UK.

[3] Calm, J.M., The next generation of refrigerants – historical review, considerations, and outlook. *Int. J. Refrig*. 2008, 31, 1123–1133.

[4] Calm, J.M.; Hourahan G.C.; Refrigerant Data Update. *HPAC Eng.* 2007, 54–64.

[5] Ren, J. L. Development course of refrigerants. *Ref. AC.* 2009, 9 (3), 41–44.

[6] Calm, J.M. Toxicity Data to Determine Refrigerant Concentration Limits. *ARTI Report DOE/CE/23810-110*, 2000.

[7] Briley; George, C. A history of refrigeration. *ASHRAE J.* 2004, 46 (11), 31–34.

[8] Nielsen, O. J.; Javadi, M. S.; Sulbaek Andersen, M. P.; Hurley, M. D.; Wallington, T. J.; Singh, R. Atmospheric chemistry of $CF_3CF{=}CH_2$: Kinetics and mechanisms of gas-phase reactions with Cl atoms, OH radicals, and O_3. *Chem. Phys. Lett.* 2017, 433, 18-22.

[9] Gutman E. E.; Semiconductor Gas Sensors and Problems of the Earth's Ozono-sphere. *Sensors and Actuators B*. 1995, 23: 209–214.

[10] Environmental Effects of Ozone Depletion and Its Interactions with Climate Change: 2010 Assessment. *UNEP*, 2010.

[11] Climate Change 1995: The Science of Climate Change. Houghton, J.; Meira Filho, L.; Callander, B.; Harris, N.; Kattenberg, A.; Maskell, K. Cambridge University Press: New York, 1996.

[12] Fuglestvedt, J. S.; Berntsen, T. K.; Godal, O.; Sausen, R.; Shine,K. P.; Skodvin, T. Metrics of climate change: Assessing radiative forcing and emission indices. *Clim. Change* 2003, 58, 267−331.

[13] Manning, M.; Reisinger, A. Broader perspectives for comparing different greenhouse gases. *Phil. Trans. R. Soc. A* 2011, 369, 1891−1905.

[14] Designation and Safety Classification of Refrigerants. *ANSI/ASHRAE Standard* 34-2007. 2008.

[15] Steven, B. J. HFOs: New, low global warming potential refrigerants. *ASHRAE J.* 2009, 22–29.

[16] Brown, J. S.; Zilio, C.; Cavallini, A. The fluorinated olefin R-1234ze(Z) as a high-temperature heat pumping refrigerant. *Int. J. Refrig.*, 2009, 32(6), 1412–1422.

[17] Mukhopadhyay, S.; Nair, H.K.; Tung, H.S.; Van Der Puy, M. Process for synthesis of 1,3,3,3-tetrafluoropropene. *U.S. Patent*, 2008, 7, 345, 209

[18] Kayukawa, Y.; Tanaka, K.; Kano, Y.; Fujita, Y.; Akasaka, R.; Higashi, Y. Experimental evaluation of the fundamental properties of low-GWP refrigerant R-1234ze(Z). *Int. J. Refrig.* 2012, 35, 1003.

[19] Raabe, G. Molecular modeling of fluoropropene refrigerants. *J. Phys. Chem.* 2012, 116 (19), 5744-5751.

[20] Panagiotopoulos, A. Z. Direct determination of phase coexistence properties of fluids by Monte Carlo simulation in a new ensemble. *Mol. Phys.* 1987, 61, 813-826.

[21] Fedele, L.; Di Nicola, G.; Brown, J. S.; Bobbo, S.; Zilio, C. Measurements and correlations of cis-1,3,3,3,-tetrafluoroprop-1-ene (R1234ze(Z)) saturation pressure. *Int. J. Thermophys.* 2014, 35, 1-12.

[22] Fedele, L.; Brown, J. S.; Di Nicola, G.; Bobbo, S.; Scattolini, M. Measurements and correlations of cis-1,3,3,3,-tetrafluoroprop-1-ene (R1234ze(Z)) subcooled liquid density and vapor-phase PvT. *Int. J. Thermophys.* 2014, 35, 1415-1434.

[23] Higashi, Y.; Hayasaka, S.; Shirai, C.; Akasaka, R. Measurements of PρT properties, vapor pressures, saturated densities, and critical parameters for R1234ze(Z) and R245fa. *Int. J. Refrig.* 2015, 52, 100-108.

[24] Okazaki, S.; Higashi, Y.; Takaishi, Y.; Uematsu, M.; Watanabe, K. Procedures for

determining the critical parameters of fluids. *Rev. Sci. Instrum.* 1983, 54, 21-25.

[25] Higashi, Y. Critical parameters for HFC134a, HFC32 and HFC125. *Int. J. Refrig.* 1994, 17, 524-531.

[26] Tanaka, K. Measurements of vapor pressure and saturated liquid density for HFO-1234ze(E) and HFO-1234ze(Z). *J. Chem. Eng. Data*, 2016, 61, 1645-1648.

[27] Di Nicola, G.; Polonara, F.; Santori, G. Saturated pressure measurements of 2,3,3,3-tetrafluoroprop-1-ene (HFO-1234yf). *J. Chem. Eng. Data* 2010, 55, 201-204.

[28] Di Nicola, G.; Polonara, F.; Ricci, R.; Stryjek, R. PVTx measurements for the R116 + CO2 and R41 + CO2 systems. New isochoric apparatus. *J. Chem. Eng. Data* 2005, 50, 312–318.

[29] Tanaka, K.; Higashi, Y. Thermodynamic properties of HFO-1234yf (2,3,3,3-tetrafluoropropene). *Int. J. Refrig.* 2010, 33, 474-479.

[30] Di Nicola, C.; Di Nicola, G.; Pacetti, M.; Polonara, F.; Santori, G. P-V-T behavior of 2,3,3,3-tetrafluoroprop-1-ene (HFO-1234yf) in the vapor phase from (243 to 373) K. *J. Chem. Eng. Data* 2010, 55, 3302-3306.

[31] Richter, M.; Mclinden, M. O.; Lemmon, E. W. Thermodynamic properties of 2,3,3,3-tetrafluoroprop-1-ene (R1234yf): vapor pressure and P-ρ-T measurements and an equation of state. *J. Chem. Eng. Data* 2011, 56, 3254-3264.

[32] McLinden, M. O.; Losch-Will, C. Apparatus for wide-ranging,high-accuracy fluid (P-ρ-T) measurements based on a compact two-sinker densimeter. *J. Chem. Thermodyn.* 2007, 39, 507–530.

[33] Fedele, L.; Brown, J. S.; Colla, L.; Ferron, A.; Bobbo, S.; Zilio, C. Compressed liquid density measurements for 2,3,3,3-tetrafluoroprop-1-ene (R1234yf). *J. Chem. Eng. Data*, 2012, 57 (2), 482-489.

[34] Klomfar, J.; Souckova, M.; Patek, J. Liquid-phase P-ρ-T data for 2,3,3,3-tetrafluoroprop-1-ene (R-1234yf) and 1,1,2,3,3,3-hexafluoroprop-1-ene (R-1216) at temperatures from (208 to 353) K under pressures up to 40 MPa. *J. Chem. Eng. Data*

2012, 57, 3283-3289.

[35] Klomfar, J.; Souckova, M.; Patek, J. Experimental′ p−ρ−T data for 1-butyl-3-methylimidazolium tetrafluoroborate at temperatures from (240 to 353) K and pressure up to 60 MPa. *J. Chem. Eng. Data* 2011, 56, 426−436.

[36] Yang, Z. Q.; Kou, L. G.; Mao, W.; Lu, J.; Zhang, W.; Lu, Jian. Experimental study of saturated pressure measurements for 2,3,3,3-tetrafluoropropene (HFO-1234yf) and 2-chloro-1,1,1,2-tetrafluoropropane (HCFC-244bb). *J. Chem. Eng. Data* 2014, 59, 157-160.

[37] Hu, P.; Cai, X. D.; Chen, L. X.; Xu, H.; Zhao, G. PVT properties of 2,3,3,3-tetrafluoroprop-1-ene (HFO-1234yf) in the gaseous phase. *J. Chem. Eng. Data* 2017, 62, 3353-3359.

[38] Wagner, W.; Kleinrahm, R. Densimeters for very accurate density measurements of fluids over large ranges of temperature, pressure, and density. Metrologia, 2004, 41, 24−39.

[39] Kamiaka, T.; Dang, C.; Hihara, E. Vapor-liquid equilibrium measurements for binary mixtures of R1234yf with R32, R125, and R134a. *Int. J. Thermophys.* 2013, 36, 965-971.

[40] Akasaka, R.; Tanaka, K.; Higahsi, Y. Measurements of saturated densities and critical parameters for the binary mixture of 2,3,3,3-tetrafluoropropene (R-1234yf) + difluoromethane (R-32). *Int. J. Refrig.* 2013, 36 (4), 1341-1346.

[41] Hu, P.; Chen, L. X.; Zhu, W. B.; Jia, L.; Chen, Z. S. Vapor-liquid equilibria for the binary system of 2,3,3,3-tetrafluoroprop-1-ene (HFO-1234yf) + 1,1,1,2,3,3,3-heptafluoropropane (HFC-227ea). *Fluid. Phase. Equlib.* 2014, 379, 59-61.

[42] Juntarachat, N.; Valtz, A.; Coquelet, C.; Privat, R.; Jaubert, J. N. Experimental measurements and correlation of vapor-liquid equilibrium and critical data for the CO_2 + R1234yf and CO_2 + R1234ze(E) binary mixtures. *Int. J. Refrig.* 2014, 47, 141-152.

[43] Coquelet, C.; Chareton, A.; Valtz, A.; Baba-Ahmed, A.; Richon, D. Vapor-liquid equilibrium data for the azeotropic difluoromethane + propane system at temperatures from 294.83 to 343.26 K and pressures up to 5.4 MPa. *J. Chem. Eng. Data* 2003, 48, 317-

323.

[44] Chen, L. X.; Hu, P.; Zhu, W. B.; Jia, L.; Chen, Z. S. Vapor-liquid equilibria of fluoroethane (HFC-161) + 2,3,3,3-tetrafluoroprop-1-ene (HFO-1234yf). *Fulid Phase Equilib.* 2015, 392, 19-23.

[45] Chen, Q.; Qi, H.; Zhang, S.; Hong, R.; Chen, G. An experimental study of PVTx properties in the gas phase for binary mixtures of HFO-1234yf and HFC-134a. *Fluid Phase Equilib.* 2015, 385, 25-28.

[46] Yang, Z. Q.; Kou, L. G.; Han, S.; Li, C.; Hao, Z. J.; Mao, W.; Zhang, W.; Lu, J. Vapor-liquid equilibria of 2,3,3,3-tetrafluoropropene (HFO-1234yf) + 1,1,1,2,2-pentafluoropropane (HFC-245cb) system. *Fluid Phase Equilib.* 2016, 427, 390-393.

[47] Higashi, Y. Measurements of thermodynamic properties for the 50 mass% R134yf + 50 mass% R1234ze(E) blend. *Sci. Technol. Built. En.* 2016, 22 (8), 1185-1190.

[48] Hu, X. Z.; Yang, T.; Meng, X. Y.; Bi, S. S.; Wu, J. T. Vapor liquid equilibrium measurements for difluoromethane (R32) + 2,3,3,3-tetrafluoroprop-1-ene (R1234yf) and fluoroethane (R161) + 2,3,3,3-tetrafluoroprop-1-ene (R1234yf). *Fluid Phase Equilib.* 2017, 438, 10-17.

[49] Hu, X. Z.; Meng, X. Y.; Wu, J. T. Isothermal vapor liquid equilibrium measurements for difluoromethane (R32) + trans-1,3,3,3-tetrafluoropropene (R1234ze(E)). *Fluid Phase Equilib.* 2017, 431, 58-65.

[50] Cai, X. D.; Zhang, N.; Chen, L. X.; Hu, P.; Zhao, G.; Liu, M. H. Gaseous PVTx measurements of HFO-1234yf + HFC-32 binary mixture by single-sinker magnetic suspension densimeter. *Fluid Phase Equilib.* 2018, 460, 119-125.

[51] Tanaka, T.; Okamoto, H.; Ueno, K.; Irisawa, J.; Otsuka, T.; Noigami, T.; Dobashi, R. Development of a new low-GWP refrigerant composed of HFO-1123(trifluoroethylene). *AIChE Annual Meeting*, 2014.

[52] Kayukawa, Y.; Kano, Y.; Fujita, Y.; Hashimoto, M.; Fukushima, M. Measurements for vapor pressures and PVT properties for low-GWP refrigerant, HFO-1123, by a

magnetic levitation densimeter. *JSRAE Annual Conference*, 2015, Tokyo, Japan.

[53] Fukushima, M.; Hayamizu, H.; Hashimoto, M. Thermodynamic properties of low-GWP alternative refrigerants. *24th IIR International Congress of Refrigeration*, 2015, Yokohama, Japan.

[54] Higashi, Y.; Akasaka, R. Measurements of thermodynamic properties for R1123 and R1123+R32 mixture. *International Refrigeration and Air Conditioning Conference*, 2016.

[55] Raabe, G. Molecular simulation studies in hydrofluoroolefine (HFO) working fluids and their blends. *Sci. Technol. Built. EN.* 2016, 22, 1077-1089.

[56] Higashi, Y.; Sakoda, N.; Amirul Islam, Md.; Yanaka, Y.; Koyama, S.; Akasaka, R. Measurements of saturation pressures for trifluoroethene (R1123) and 3,3,3-trifluoropropene (R1243zf). *J. Chem. Eng. Data* 2018, 63(2), 417-421.

[57] Burnett E.S. Compressibility determinations without volume measurements. Apparatus to determine compressibility with pressure and temperature measurements. *J. appl. Mech.* 1936.

[58] Sakoda, N.; Shindo, K.; Motomura, K.; Shinzato, K.; Kohno, M.; Takata, Y.; Fujii, M. Burnett PVT measurements of hydrogen and the development of a virial equation of state at pressures up to 100 MPa. *Int. J. Thermophys.* 2012, 33, 381-395.

[59] Perston-Thomas, H. The international temperature scale of 1990 (ITS-90). *Metrologia* 1990, 27,

[60] ISO; IEC; OIML; BIPM. Guide to the expression of uncertainties in measurement (Switzerland: ISO). 1993.

[61] Sakoda, N.; Jiang, S. H.; Kohno, M.; Koyama, S.; Higashi, Y.; Takata, Y. Gaseous PVT property measurements of cis-1,3,3,3-tetrafluoropropene. *J. Chem. Eng. Data* 2017, 62 (7), 2178-2182.

[62] Shimawaki, S.; Fujii, K.; Higashi, Y. Precise Measurements of the vapor-liquid equilibria (VLE) of HFC-32/134a mixtures using a new apparatus. *Int. J. Thermophys.* 2002, 23 (3), 801-808.

[63] Kayukawa,Y.; Fujii, K.; Higashi,Y. Vapor-liquid equilibrium (VLE) properties for the binary system propane (1) + n-butane (2) and propane (1) + isobutene (3). *J. Chem. Eng. Data* 2005, 50, 579-582.

[64] Ortiz-Vega, D.O.; Hall, K.R.; Holste, J.C.; Arp, V.D.; Lemmon, E.W. A new wide range equation of state for helium-4. Doctoral dissertation, *J. Phys. Chem. Ref. Data*, 2013.

[65] Lemmon, E. W.; Huber, M. L.; McLinden, M. O. NIST Standard Reference Database 23, NIST Reference Fluid Thermodynamic and Transport Properties Database (REFPROP): Version 9.1, Standard Reference Data, National Institute of Standards and Technology: Gaithersburg, MD. 2013.

[66] Span, R.; Lemmon, E. W.; Jacobsen, R. T; Wagner, W.; Yokozeki, A. A reference equation of state for the thermodynamic properties of nitrogen for temperatures from 63.151 to 1000 K and pressures to 2200 MPa. *J. Phys. Chem. Ref. Data* 2000 29, 1361-1433.

[67] Tillner-Roth, R.; Baehr, H. D. An international standard formulation of the thermodynamic properties of 1,1,1,2-tetrafluoroethane (HFC-134a) for temperatures from 170 K to 455 K at pressures up to 70 MPa. *J. Phys. Chem. Ref. Data* 1994, 23, 657-729.

[68] Akasaka, R.; Higashi, Y.; Miyara, A.; Koyama, S. A fundamental equation of state for cis-1,3,3,3-tetrafluoropropene (R-1234ze(Z)). *Int. J. Refrig.* 2014, 44, 168-176.

[69] Tillner-Roth, R.; Yokozeki, A. An international standard equation of state for difluoromethane (R-32) for temperatures from the triple point at 136.34 K to 435 K and pressures up to 70 MPa. *J. Phys. Chem. Ref. Data* 1997, 26(6), 1273-1328.

[70] Richter, M.; McLinden, M.O.; Lemmon, E.W. Thermodynamic properties of 2,3,3,3-tetrafluoroprop-1-ene (R1234yf): Vapor pressure and p-ρ-T measurements and an equation of state. *J. Chem. Eng. Data* 2011, 56(7), 3254-3264.

[71] Kunz, O.; Wagner, W. The GERG-2008 wide-range equation of state for natural

gases and other mixtures: An expansion of GERG-2004. *J. Chem. Eng. Data* 2012, 57, 3032-3091.

[72] Akasaka, R. Thermodynamic property models for the difuoromethane (R-32) + trans-1,3,3,3-tetrafluoropropene (R-1234ze(E)) and difluoromethane + 2,3,3,3-tetrafluoropropene (R-1234yf) mixtures. *Fluid Phase Equilib.* 2013, 358, 98-104.

[73] Akasaka, R. A thermodynamic property model for difluoromethane (R-32) and trifluoroethylene (R-1123) mixtures. ATPC, 2016.

[74] Akasaka, R.; Fukushima, M.; Lemmon, E.W. A Helmholtz energy equation of state for trifluoroethylene (R-1123). International Refrigeration and Air Conditioning Conference at Purdue, July 11-14

[75] Pend, D., Robinson, D.B. A new two-constant equation of state. *Ind. Eng. Chem.* 1976, 15, 59-64.

[76] Lemmon, E.W., Jacobsen, R.T. Equations of state for mixtures of R-32, R-125, R-134a, R-143a, and R-152a. *J. Phys. Chem. Ref. Data* 2013, 33 (2), 593-620

Acknowledgement

I would like to take this opportunity to express my gratitude to all the people who have ever helped me during my doctoral period. Firstly, my sincere thanks and appreciations go first to my supervisor, ***Professor Takata***, for taking me in his laboratory as a Ph.D. student. It has been a great privilege and joy to study under his guidance and supervision.

I am also deeply indebted to ***Professor Sakoda***, for his instructive advice and useful suggestions on my experiments during the seminar. Also I must thank him for his help and patience on my thesis. He spent much time reading through each draft and provided me with inspiring advice.

I express my deep thanks to ***Professor Higashi*** for letting me join his experiments. I express my deep appreciation to ***Ms. Shuto*** for her kind help in my study life.

I express my deep thanks to my dissertation committee members, ***Professor Kohno*** and ***Professor Higashi*** for their invaluable time and advice.

I wish to express my warm thanks to members of Thermofluid Physics Laboratory.

I would like to thank my family for their support and understanding.

Lastly, I gratefully acknowledge to Hydrogen Energy System for giving me the opportunity to work as a research assistant.

Fukuoka, June 2018

Shiheng Jiang